Cultivation of a three-dimensional adipose tissue engineered construct modeling the inflammatory phenotypes found in obese patients.

A thesis submitted by

Adam Zieba

in partial fulfillment of the requirements for the degree of

Master of Science

in

Biomedical Engineering

TUFTS UNIVERSITY

May 2017

Research Adviser: Professor David L. Kaplan, PhD

Abstract

Obesity promotes the development of a variety of diseases including type 2 diabetes, cardiovascular disease, fatty liver, and cancer. As obesity is characterized by a chronic state of low-grade inflammation distinguished by immune cell infiltration into the adipose tissue, a model demonstrating this inflammatory state is needed to better understand the disease itself as well as how it affects different patients. Utilizing a 3D tissue-engineered *in vitro* adipose construct integrating a 3D silk fibroin porous scaffold and the multiple cell types found in adipose tissue, an induced inflammatory model was created by the addition of THP-1 derived macrophages. The model demonstrated increased cell proliferation, higher rates of lipolysis, and an upregulation of leptin production in a patient specific manner. The results demonstrate the successful development of an inflammatory state and highlight the patient specific response to inflammatory conditions.

Acknowledgements

Committee Members:
David Kaplan, PhD
Kyongbum Lee, PhD
Lauren Black, PhD

Kaplan Laboratory:

Adipose Tissue Group
Rosalyn Abbott-Beauregard, PhD
Sarah Lightfoot-Vidal
Rebecca Wang

The seemingly endless members of the Kaplan Lab that helped me out with advice and/or motivation

Milva Ricci
Laura Suarez

Friends and Family

Table of Contents

Abstract ii
Acknowledgements iii
Table of Contents iv
List of Tables vi
List of Figures vii
List of Abbreviations ix
1. Introduction 1
1.1. Societal Impact of Obesity 1
1.1.1. Causes and Health Risks 2
1.1.2. Economic Impact 3
1.2. White Adipose Tissue Function 3
1.3. Macrophages 5
1.3.1. THP-1 Differentiation and Polarization 6
1.4. Adipose Tissue Inflammation and Macrophages 7
1.5. Acute and Chronic Inflammation 10
1.6. Tissue Engineering 11
1.6.1. 2D vs 3D Cell Culture 13
1.7. Silk-Based Scaffolds for Tissue Engineering 13
1.8. Introduction to Adipose Tissue Engineering 15
1.8.1. Efforts to Model Obesity 17
1.9. Coherent anti-Stokes Raman Scattering (CARS) Microscopy 19
2. Rational Project Design 22
2.1 Motivation and Problem Statement 22
2.2 Hypothesis 22
2.3 Aim 1: Confirm THP-1 monocytes can be differentiated into macrophages and polarized towards M1 and M2 states 23
2.4. Aim 2: Simulate the immune cell infiltration seen in obesity in adipose constructs 24
2.5. Aim 3: Induce an acute inflammatory response in adipose constructs 25
2.6. Innovation 26
3. Materials and Methods 27
3.1. Materials List 27
3.1.1. Cell Culture Materials 27
3.1.2. Assay Materials 27

3.1.3. Other Materials 28
3.2. THP-1 Differentiation and Polarization Study 28
3.3. Silk Processing 29
3.4. Silk Scaffold Preparation 30
3.5. Primary Lipoaspirate Isolation and Cell Seeding 32
3.6. Macrophage Infiltration Study 33
3.7. LPS Acute Inflammation Study 33
3.8 Assays 33
3.8.1. RT-qPCR 33
3.8.2. Picogreen DNA Quantification Assay 35
3.8.3. Glycerol Secretion Quantification Assay 36
3.8.4. Leptin Secretion Enzyme-Linked Immunosorbent Assay (ELISA) 36
3.8.5. Intracellular Triglyceride Quantification Assay 37
3.9. Immunohistochemistry 37
3.10 Statistical Analysis 38
4. Results 39
4.1. Aim 1. Confirming THP-1 monocytes can be differentiated into macrophages and polarized towards M1 and M2 states 39
4.1.1. Imaging 39
4.1.2. Gene Expression 41
4.2. Aim 2: Simulating the immune cell infiltration seen in obesity in adipose constructs 43
4.2.1. DNA Content 43
4.2.2. Triglyceride Content 46
4.2.3. Leptin Secretion 48
4.2.4. Glycerol Secretion 51
4.2.5. Confocal Imaging 53
4.3. Aim 3: Inducing an acute inflammatory response in adipose constructs 56
4.3.1 DNA Content 56
4.3.2. Glycerol Secretion 56
5. Discussion 58
6. Conclusions and Future Directions 63
6.1. Future Directions 63
References 66

List of Tables

Table 1. Summary of the various biomedical applications of silk fibroin and associated morphologies

Table 2. Summary of approaches to induce the inflammatory state of obesity *in vitro*.

Table 3. List of primers used for RT-qPCR

Table 4. Known information on patient samples used.

List of Figures

Figure 1. Estimates of the percentage of children that are overweight (including obese) in various countries

Figure 2. The organization of white adipose tissue. (a) The different cell types present in white adipose tissue. (b) The composition of a unilocular white adipocyte

Figure 3. Schematic highlighting the different stimuli involved in macrophage polarization and the different functions of the polarizations

Figure 4. The influence of weight gain on adipose tissue. As obesity develops, inflammation and progressive macrophage recruitment increases

Figure 5. Schematic illustrating the crosstalk between cells in the adipose tissue as a result of obesity and the recruitment of macrophages

Figure 6. Development and applications of tissue engineering

Figure 7. Theory behind CARS microscopy. The schematic highlights the differences between Raman spectroscopy (top) and CARS (bottom) and the need for both a Pump and Stokes beam in CARS spectroscopy

Figure 8. Schematic summarizing the differentiation and polarization process described in Aim 1.

Figure 9. Schematic summarizing the experimental design of the simulated immune cell infiltration described in Aim 2.

Figure 10. Schematic summarizing the experimental design of acute inflammation stimulation described in Aim 3.

Figure 11. Schematic illustrating the process of attaining an aqueous silk fibroin solution from *Bombyx mori* silk cocoons

Figure 12. Schematic illustrating the process of fabricating silk sponge scaffolds from lyophilized silk solution.

Figure 13. Schematic describing the sandwich ELISA process

Figure 14. Brightfield images of THP-1 macrophages taken with a light microscope after the differentiation and polarization process.

Figure 15. Fluorescent images of the THP-1 macrophages taken with a confocal microscope after the differentiation and polarization process.

Figure 16. Gene expression of THP-1 macrophages after polarization

Figure 17. DNA content after simulation of immune cell infiltration

Figure 18. Triglyceride content normalized by DNA content after simulation of immune cell infiltration

Figure 19. Leptin secretion normalized by DNA content after simulation of immune cell infiltration

Figure 20. Glycerol secretion normalized by DNA content after simulation of immune cell infiltration

Figure 21. Fluorescent images of the adipose constructs using samples from Patient 2 taken with a confocal microscope at four different timepoints

Figure 22. Fluorescent images of the adipose constructs using samples from Patient 3 taken with a confocal microscope at four different timepoints

Figure 23. DNA content and normalized glycerol secretion after LPS stimulation.

List of Abbreviations

BMI (Body mass index)
CARS (coherent anti-Stokes Raman scattering)
CD68 (cluster of differentiation 68)
DAPI (4',6-diamidino-2-phenylindole0
ECM (extracellular matrix)
HASCs (human adipose-derived stem cells)
HFIP (hexafluoroisopropanol)
IFN-γ (interferon gamma)
IL-1β (interleukin-1 beta)
IL-2 (interleukin-2)
IL-4 (interleukin-4)
IL-6 (interleukin-6)
IL-8 (interleukin-8)
IL-13 (interleukin-13)
iNOS (induced nitric oxide synthase)
LPS (lipopolysaccharide)
MCP-1 (monocyte chemoattractant protein-1)
MRC-1 (mannose receptor c-type 1)
NaCl (sodium chloride)
PAMPS (pathogen-associated molecular patterns)
PMA (phorbol 12-myristate 13-acetate)
RT-qPCR (Quantitative reverse transcription polymerase chain reaction)
SGBS (Simpson-Golabi-Behmel syndrome)
TNF-α (tumor necrosis factor alpha)
WAT (white adipose tissue)
2D (two-dimensional)
3D (three-dimensional)

1. Introduction

1.1. Societal Impact of Obesity

Obesity is one of society's most pervasive diseases desperate for further exploration of strategies to both treat and prevent it. Obesity is characterized as a chronic state of low-grade inflammation distinguished by progressive immune cell infiltration into adipose tissues (Bai and Sun, 2015). Although not perfect, the standard measure of obesity is body mass index (BMI, (weight in kg)/(height in m)^2). Obesity is defined by having a BMI greater than 30 kg/m^2 (Lehnert et al., 2013). In the United States, specifically, obesity affects over a third of adults (34.9%) as well as 16.9% of children (Ogden et al., 2014).

The US is not the only country with high rates of obesity as the obesity epidemic has been steadily increasing its prevalence across the globe. Although primarily beginning in wealthier countries, middle-income and low-income countries have also seen a widespread increase in incidences of obesity (Swinburn et al., 2011). In 2008, 1.46 billion adults were overweight while 502 million were obese. Even more frightening, about 170 million children are estimated to be either overweight or obese (Swinburn et al., 2011). **Figure 1** illustrates the trends affecting children of a select group of countries.

Socioeconomic status is another factor influencing obese populations. Interestingly, in poorer countries, a higher socioeconomic status and closer proximity to urban areas increases the likelihood of becoming obese (Swinburn et al., 2011). However, wealthier countries exhibit the reverse effect as a lower socioeconomic status and closer proximity to rural areas result in higher incidences of obesity (Swinburn et al., 2011). This further demonstrates the need for continued research of the disease.

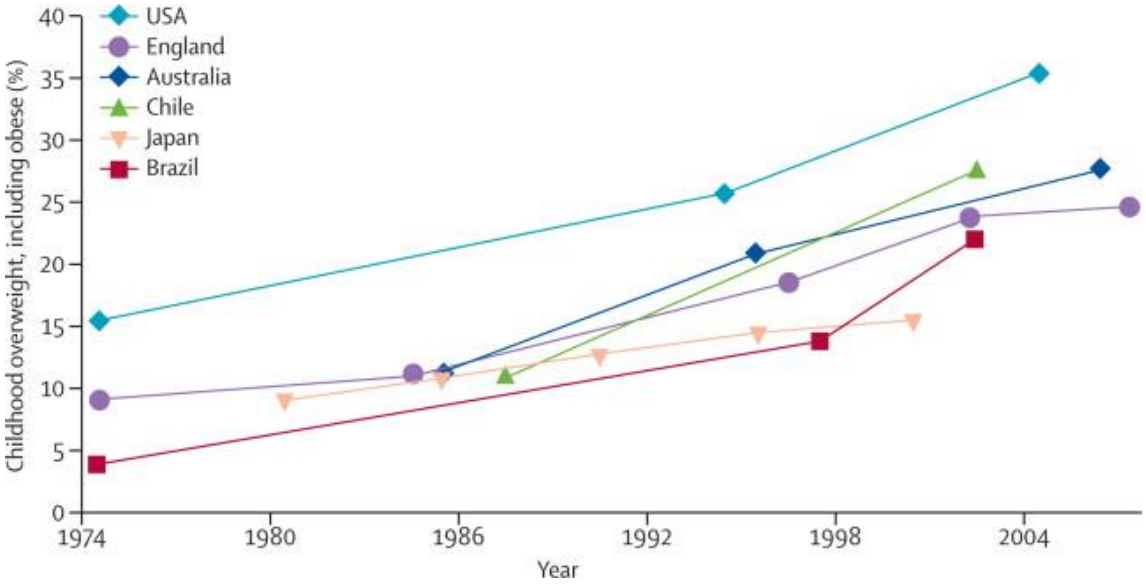

Figure 1. Estimates of the percentage of children that are overweight (including obese) in various countries (Swinburn et al., 2011).

1.1.1. Causes and Health Risks

Many factors are thought to contribute to the development of obesity. Obesity is characterized by the accumulation of adipose tissue due to an energy imbalance in the body. Fat is stored if a person intakes more energy than they expend (Kopelman, 2007). Diets high in fats and sugars promote this energy imbalance and leading to weight gain. However, evidence shows that individuals can be genetically predisposed to obesity (Kopelman, 2007). Other evidence shows exposure to environmental chemicals, or "obesogens," *in utero* may also make individuals more prone to weight gain (Wang et al., 2016).

Obesity is highly associated with an increased risk of developing type 2 diabetes, cardiovascular disease, nonalcoholic fatty liver, and osteoarthritis (Ahima and Lazar, 2013). It has also been shown to contribute to the development of hypertension, elevated plasma insulin levels and insulin resistance, hyperglycemia, and hyperlipidemia (Kopelman, 2007). Obesity, marked by a BMI greater than 30 kg/m^2, predisposes the population to an increased mortality rate due cardiovascular disease, diabetes, cancer, and other diseases (Kopelman, 2007).

Therefore, increased incidences of obesity will consequently incite greater incidences of a myriad of other diseases.

1.1.2. Economic Impact

As obesity affects such a large portion of the population, the economic liability it imposes is staggering. One study suggests that when adding together direct costs and various indirect costs, the annual costs associated with obesity reach upwards of $215 billion (Hammond and Levine, 2010). In 2005, about 20% of United States healthcare expenditures ($190 billion) went to direct costs of medical care associated with obesity (Lehnert et al, 2013). In addition to direct costs, indirect costs like decreased workforce productivity, whether it be decreased productivity while working or the inability to work, can match or even surpass directs costs (Lehnert et al., 2013). New methods to treat and prevent obesity will reduce its economic burden on healthcare in addition to increasing quality of life.

1.2. White Adipose Tissue Function

White adipose tissue's (WAT) primary function was always thought to be as an energy reserve depot to be used in cases of food deprivation (Trayhurn and Beattie, 2001). However, WAT has also emerged as an endocrine organ that secretes adipokines and cytokines affecting functions of other tissue systemically (Fantuzzi, 2005). WAT has mesenchymal origins and consists of connective tissue, immune cells, blood vessels, sympathetic innervation, stem cells (preadipocytes), and adipocytes (**Figure 2a**). The adipocytes perform WAT's primary function of fat intake, storage, and mobilization (Bolsoni-Lopes et al., 2015).

Energy is stored in the form of triglycerides, neutral lipids that consist of three fatty acids esterified to the carbon backbone of a glycerol molecule. Adipocytes store triglycerides in large,

unilocular lipid droplets that take up about 90% of the cytoplasm (**Figure 2b**) (Bolsoni-Lopes et al., 2015). The amount of triglycerides relies on the proportion of lipogenesis (synthesis and storage of triglycerides) and lipolysis (hydrolysis of triglycerides into glycerol and fatty acids to release energy) (Bolsoni-Lopes et al., 2015). In the case of obesity, increased basal lipolysis rates have shown to contribute to the development of insulin resistance and impaired responsiveness to stimulated lipolysis (Duncan et al., 2007).

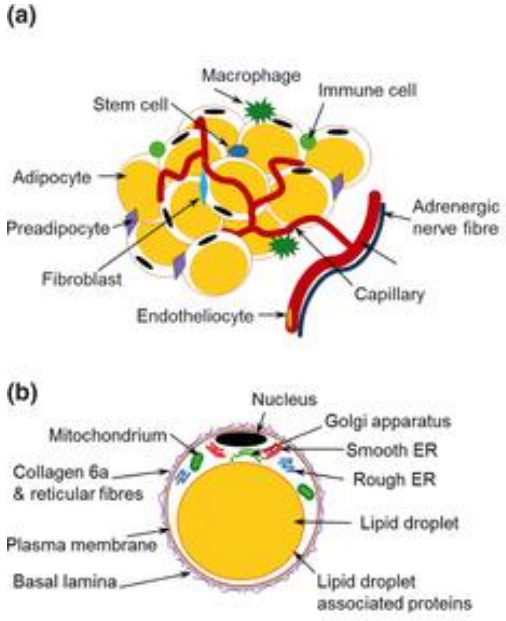

Figure 2. The organization of white adipose tissue. (a) The different cell types present in white adipose tissue. (b) The composition of a unilocular white adipocyte (Wronksa and Kmiec, 2012).

As an endocrine organ, WAT secretes various proinflammatory and anti-inflammatory factors. Cytokines and chemokines secreted include tumor necrosis factor alpha (TNF-α), interleukin 6 (IL-6), monocyte chemoattractant protein-1 (MCP-1), and others (Fantuzzi, 2005). Secreted adipokines include leptin, adiponectin, resistin, and visfatin (Fantuzzi, 2005). Specifically, leptin is a proinflammatory hormone involved in innate and adaptive immunity that exhibits increased production in obese individuals (Bai and Sun, 2015). Adiponectin, on the

other hand, suppresses lipid accumulation and has anti-inflammatory effects (Bai and Sun, 2015).

1.3. Macrophages

Macrophages are phagocytic immune cells. Human macrophages are typically described by the two polarized states: M1 macrophages (classically activated macrophages) and M2 macrophages (alternatively activated macrophages) (**Figure 3**) (Chanput et al., 2013). The M1 phenotype results from exposure to pathogen associated molecular patterns (PAMPS) or Th1 cytokines like interferon gamma (IFN-γ) and tumor necrosis factor alpha (TNF-α). The typical M1 phenotype can be identified by the increased production of pro-inflammatory cytokines such as TNF-α, interleukin-1 beta (IL-1β), IL-6, interleukin-8 (IL-8), and interleukin-12 (IL-2) (Chanput et al., 2013). On the other hand, M2 macrophages result from responding to TH2 cytokines like interleukin-4 (IL-4) and interleukin-13 (IL-13). As opposed to the M1 macrophage's pro-inflammatory function, M2 macrophages are involved in parasite infection, tissue modeling, immunoregulation, allergy, and tumor progression (Chanput et al., 2013).

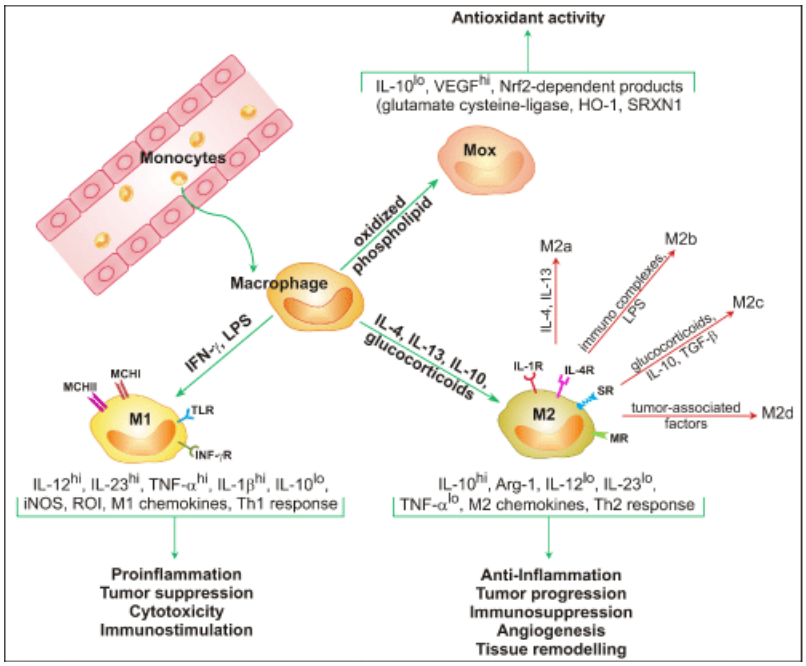

Figure 3. Schematic highlighting the different stimuli involved in macrophage polarization and the different functions of the polarizations (Fraternale et al., 2015).

1.3.1. THP-1 Differentiation and Polarization

The THP-1 cell line is a human leukemia-derived monocytic cell line that is the current standard in *in vitro* studies exploring primary human macrophage function. THP-1 cells can be stimulated using phorbol 12-myristate 13-acetate (PMA) resulting in both phenotypic and functional traits resembling primary human macrophages. Successful differentiation can be distinguished by cell adhesion (non-differentiated cells stay in suspension), cell spreading, and the ability to be stimulated by pro-inflammatory stimuli (Lund et al., 2016). The decision to use the THP-1 cell line instead of primary macrophages is common due to the natural limitations of the primary cells. Primary macrophages cannot be expanded *ex vivo* and have a very limited lifespan in culture (Lund et al., 2016). THP-1 cells, on the other hand, can grow very quickly, can be cultured up to 3 months, and can be frozen in liquid nitrogen (Chanput et al., 2014). The primary drawback in using the THP-1 cell line (along with other cell lines) is the possibility that

they will react differently when compared to normal somatic cells in in their natural environment. (Chanput et al., 2014)

Differentiating THP-1 cells to obtain the resting macrophage phenotype (M0) is widely accomplished using PMA. However, no standard protocol has been established. Lund et al. sought out to compare the range of published PMA differentiation protocols and assess their resulting phenotypes and function. The group concluded that the results varied significantly and were reliant on the concentration of PMA and the resting period after PMA exposure. The study found that higher concentrations of PMA led to an increased stimulation to an inflammatory stimulus but also increased base inflammatory gene expression. The study concluded that to obtain macrophages that were able to induce a measurable response while also limiting the inflammatory response from the PMA itself, exposure to a concentration of 25 nM PMA for 48 hours followed by a 24-hour rest period should be used to induce a consistent phenotype of THP-1 macrophages (Lund et al., 2016). Hence, in the following experiments, this protocol was used. THP-1 macrophages have also shown the ability to polarize towards the M1 and M2 phenotypes. Exposure to lipopolysaccharide (LPS) and IFNγ polarize resting macrophages towards the M1 phenotype while exposure to IL-4 and IL-13 polarize resting macrophages towards the M2 phenotype (Chanput et al., 2013 and Genin et al., 2015).

1.4. Adipose Tissue Inflammation and Macrophages

As previously mentioned, obesity is characterized by the state of chronic, low-grade inflammation in the adipose tissue. In trying to understand the mechanisms behind obesity and its related diseases, alterations in both the metabolic and inflammatory pathways are encountered (Wellen and Hotamisligil, 2003). Adipose tissue itself has been shown to produce proinflammatory factors and is a target of inflammatory processes. In particular, studies reveal

that visceral white adipose tissue develops a proinflammatory state in obese phenotypes. In addition, accumulation of macrophages influences the enhanced fat mass-derived production of chemokines (Curat et al., 2006).

Multiple studies have shown macrophage infiltration into adipose tissue in obese phenotypes. One study demonstrates that in isolated adipose tissue, various proteins associated with macrophages are positively correlated with increased body mass (Weisberg et al., 2003). Additionally, it demonstrates the expression of proinflammatory cytokines (the bulk of overall TNF-α expression as well as large amounts of inducible nitric oxide synthase (iNOS) and IL-6 expression) are caused by resident adipose tissue macrophages (Weisberg et al., 2003). A separate study targeting the link between chronic inflammation and insulin resistance discovered that inflammation and macrophage-specific genes are upregulated in the white adipose tissue in obese phenotypes (Xu et al., 2003). The study also demonstrated that macrophages, unlike other immune cells like neutrophils or lymphocytes, infiltrate the adipose tissue of obese mice (Xu et al., 2003). Together, these studies indicate resident and infiltrating macrophages initiate and propagate chronic inflammation in the adipose tissue.

Macrophage recruitment could be caused by a variety of factors (**Figure 4**). It has been suggested that in obesity, adipocytes and endothelial cells secrete TNF-α which stimulates the production of MCP-1, a monocyte recruiter (Wellen and Hotamisligil, 2003). Additionally, the increased secretion of leptin eases the transport of macrophages to the adipose tissue and promotes attachment of macrophages to the endothelial cells. Size change and overcrowding of cells as well as oxidative damage caused by lipolysis can damage the endothelium prompting innate macrophage recruitment as well (Wellen and Hotamisligil, 2003).

Adipose tissue macrophages in healthy individuals tend to exhibit M2 surface markers, but data suggests that obesity promotes a transition from the M2 polarized state to the pro-inflammatory M1 state (Lumeng et al., 2007). The thought is that factors in the pro-inflammatory environment of obese adipose tissue pushes the macrophages towards the M1 state (Lumeng et al., 2007).

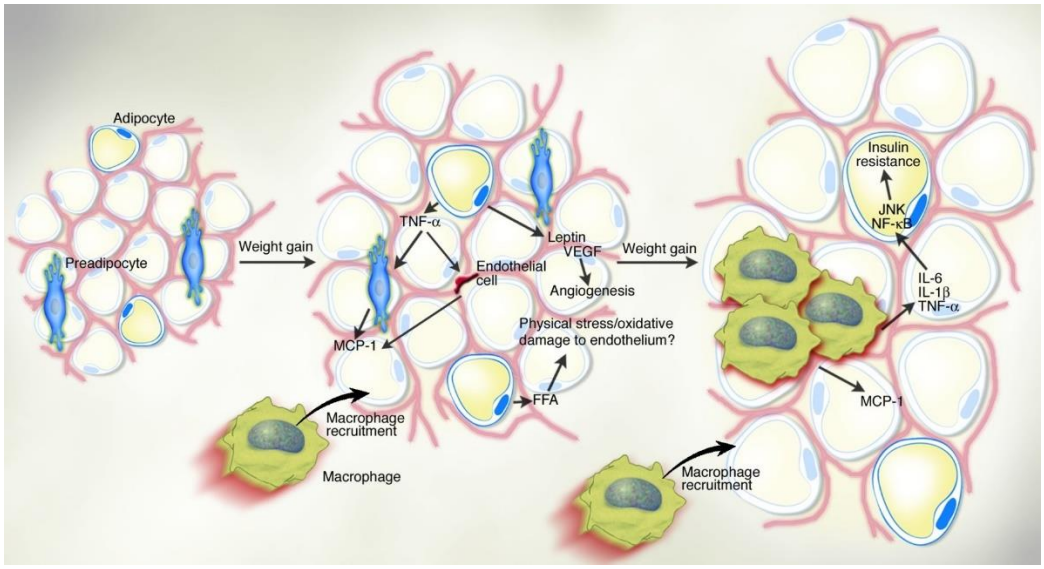

Figure 4. The influence of weight gain on adipose tissue. As obesity develops, inflammation and progressive macrophage recruitment increases (Wellen and Hotamisligil, 2003).

The chronic state of inflammation is the direct result of the crosstalk of adipocytes and macrophages. Adipocytes secrete MCP-1, TNF-α, and saturated fatty acids inducing proinflammatory pathways in resident macrophages. Activated macrophages secrete a variety of pro-inflammatory chemokines, including MCP-1, recruiting monocytes from circulation into the site of inflammation (Bai and Sun, 2015). Once recruited to the adipose tissue, the monocytes and macrophages participate in cell-to-cell signaling with adipocytes and other resident cells promoting production of pro-inflammatory adipokines (**Figure 5)**, downregulating the

production anti-inflammatory adiponectin, and maintaining the state of chronic inflammation by continuing to recruit of monocytes and macrophages (Bai and Sun, 2015).

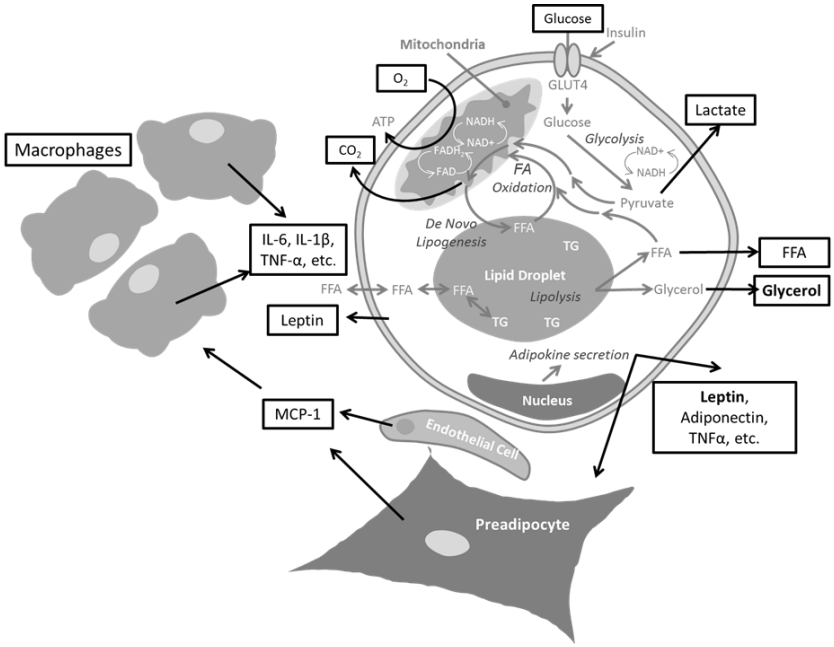

Figure 5. Schematic illustrating the crosstalk between cells in the adipose tissue as a result of obesity and the recruitment of macrophages (Wellen and Hotamisligil, 2003; Abbott et al., 2015).

1.5. Acute and Chronic Inflammation

At its fundamental level, inflammation is an innate response to stimuli and environmental conditions it deems harmful, such as infection or tissue injury. The response involves immune cells, blood vessels, and molecular mediators (Medzhitov, 2008). Inflammation is typically designated into two categories: acute inflammation and chronic inflammation (Murakami and Hirano, 2012).

The acute inflammatory response occurs at sites of infection or injury with the directed delivery of plasma and leukocytes. Tissue-resident macrophages and mast cells recognize the infection and engage in the production of proinflammatory chemokines, cytokines, vasoactive amines, elcosanoids, and products of proteolytic cascades (Medzhitov, 2008). This allows for the

influx of plasma proteins and leukocytes, which are mostly neutrophils. Once activated, neutrophils release toxins in an effort to kill their microbial targets. When acute inflammation is successful, infectious invaders are eradicated and an anti-inflammatory repair phase begins. (Medzhitov, 2008).

Among other stimuli to study acute inflammatory response, LPS has been used in a variety of studies to induce an acute inflammatory response. LPS is an active component of gram-negative bacterial cell walls that activates an acute inflammatory response (Metukuri et al., 2010). Exposure to LPS has been shown to upregulate secretion of proinflammatory cytokines in cultured keratinocytes *in vitro* as well as in human subjects *in vivo* (Ibisch et al., 2007; Dillingh et al., 2014).

Conversely, chronic inflammation is an elongated state that typically is seen in a variety of diseases such as autoimmune diseases, type 2 diabetes, and cardiovascular diseases (Medshitov, 2008). Chronic inflammation, unlike acute, is not brought about by a single event. Rather, the malfunction of tissues and the homeostatic imbalance of physiological systems induces the chronic response (Medzhitov, 2008).

1.6. Tissue Engineering

Tissue engineering can be defined as the development of biological alternatives for harvest tissues, implants, and prostheses (Yang et al., 2001). Tissue engineering depends on the interaction of cells and biomaterials, so it follows that the field relies on the science and technology from both pure biological sciences and material science engineering (Nerem and Sambanis, 1995). The field of tissue engineering explores the possibilities of manipulating cells in various ways to restore, maintain, or enhance tissues and organs. In order to engineer viable

tissue constructs *in vitro*, scaffolds made from an array of biomaterials are used to stimulate cultured cells with both physical and chemical cues to direct their growth, differentiation, and organization into sustainable three-dimensional (3D) tissues (Griffith and Naughton, 2002).

Although tissue engineering is being explored for a variety of applications (**Figure 6**), its use in developing models for disease modeling and drug screening is ideally suited (Griffith and Naughton, 2002) to create the most immediate impact. The design of *in vitro* physiologically relevant models provides an outlet to both examine disease pathology and develop molecular therapeutics (Griffith and Naughton, 2002). *In vitro* culture of tissue engineered constructs provide both flexibility and control of variables for studying various modes of infection and reactions to potential drugs.

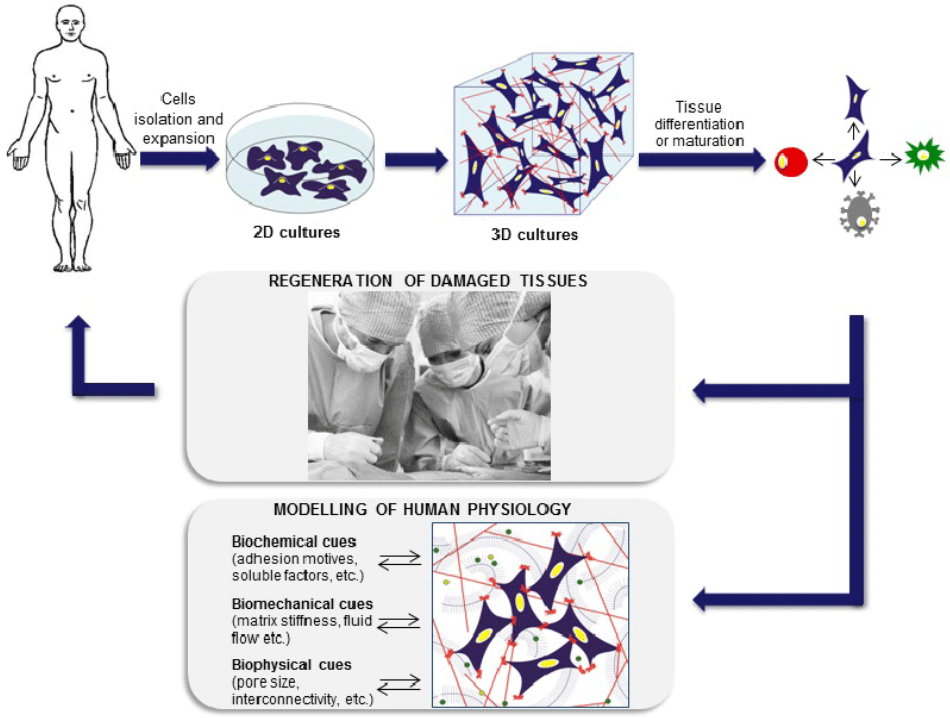

Figure 6. Development and applications of tissue engineering (Castells-Sala et al., 2013).

1.6.1. 2D vs 3D Cell Culture

In the drug discovery process, cell based assays are hugely valuable tools that are simple, fast, and cost-effective when compared to their animal testing counterpart. Researchers depend on the cellular response to drugs, compounds, and other various stimuli (Edmondson et al., 2014). However, the majority of these assays utilize two-dimensional (2D) monolayer cells as opposed to 3D constructs. Although useful, 2D cell culture has limitations as 2D monolayers fail to match the complexity of the human body (Edmondson et al., 2014).

In their natural, *in vivo* environment, cells are surrounded by other cells and an extracellular matrix. Culturing cells on flat, rigid surfaces fails to mimic this environment. Culturing cells in a 3D system more appropriately mimics *in vivo* conditions (Edmondson et al., 2014). The added dimensionality orients cell surface receptors to be able to participate in paracrine signaling while also physically constraining cells (Edmondson et al., 2014). Evidence also indicates that cells in 3D culture differ morphologically and physiologically compared to 2D cultures. In addition, 3D cultures result in cell responses more similar to *in vivo* behavior (Edmondson et al., 2014). Given these findings, 3D models are the most appropriate choice for disease modeling and drug screenings.

1.7. Silk-Based Scaffolds for Tissue Engineering

To accomplish successful three-dimensional culture, cells need an extracellular matrix (ECM) that supports their attachment and proliferation of cells. The choice of biomaterial for the ECM is crucial as it influences physical, chemical, and biological cues affecting cells. It is also beneficial for the biomaterial to degrade at a rate similar to that of new tissue formation to allow for cells to construct their own ECM. As important, biomaterials should be biocompatible to

prevent a host immune response if implanted (Vepari and Kaplan, 2007). Among others, natural biomaterials used to construct scaffolds in the field of tissue engineering include collagen, chitosan, glycosaminoglycans, and silk.

Silkworms and certain species of spiders produce the fibrous protein silk in specific epithelial cells that line the glands of the organisms. In nature, the silk fibroin polymers are employed to deliver structure in cocoon formation, nest building traps, web formation, safety lines, and egg protection (Vepari and Kaplan, 2007). At a structural level, silks consist of β-sheet structures resulting from hydrophobic domains that allow for tight packing of stacked sheets of hydrogen bonded anti-parallel chains. The combination of large hydrophobic domains separated by smaller hydrophilic domains imparts the mechanical strength and resiliency of the fibers (Vepari and Kaplan, 2007). In this work, silk fibroin is isolated from the cocoons of the domesticated silk worm, *Bombyx mori*. The fibers isolated are composed of two different proteins, a light chain and heavy chain present in a 1:1 ratio and linked by a single disulfide bond (Vepari and Kaplan, 2007).

Silk exemplifies many aspects of the ideal biomaterial. For centuries, silk has already been used as a material to make surgical sutures (Vepari and Kaplan, 2007). The protein is biocompatible, has tunable degradation and mechanical strength, induces low inflammatory and immunogenic response in tissue, can be chemically modified, and is easily sterilized (Rockwood et al, 2016). One of silk fibroins more valuable traits is its versatility; it can be produced into a number of different morphologies (**Table 1**).

Table 1. Summary of the various biomedical applications of silk fibroin and associated morphologies (Vepari and Kaplan, 2007; Rockwood et al., 2011).

Application	*Type*	*Morphology*
Tissue Engineering	Bone	HFIP and aqueous sponges Electrospun fibers Film Hydrogels
	Cartilage	HFIP and aqueous sponges Electrospun fibers Hyrdogels
	Soft tissue	HFIP and aqueous sponges Hydrogels
	Corneal	Patterned silk films
	Vascular tissues	Tubes Electrospun fibers Non-woven mats
	Cervical tissues	Aquesous sponges
	Skin	Electrospun fibers
Disease Models	Breast Cancer	HFIP and aqueous sponges
	Autosomal dominant PKD	Aqueous sponges
Implant Devices	Anterior Cruciate Ligament	Fibers
	Femur Defects	HFIP sponges
	Mandibular Defects	Aqueous sponges
Drug Delivery	Drugs	Spheres
	Growth Factors	Films
	Small Molecule	Microneedles

This work utilizes silk's ability to form porous sponge scaffolds. These sponges promote cell attachment, proliferation and migration. The size of pores in the sponges can be customized by choice of porogen size in the manufacturing process. Silk sponges can be either solvent or aqueous based depending on the needs of research (Vepari and Kaplan, 2007).

1.8. Introduction to Adipose Tissue Engineering

Due to the widespread obesity epidemic and the variety of metabolic disorders it can cause, the need for adipose tissue engineering is as prevalent as ever. Not only do these health problems impose a decreased quality of life, but they also burden patients financially. To better

understand and, in turn, combat obesity, physiologically relevant and sustainable tissue engineered constructs modeling human adipose tissue are necessary (Abbott et al., 2016). This ideal model will be able to provide a better understanding of the cause and mechanisms of different metabolic disorders as well as offer a platform to test experimental treatments without the risk of negatively affecting a patient.

The adipose tissue engineering field has not been able to produce an *in vitro* model that perfectly mimics human adipose tissue. For instance, animal cell lines like the murine 3T3-L1 line have been used. They show the ability to undergo adipogenesis in culture but fail to produce the single large lipid droplets found *in vivo* in mature adipocytes (Serlachius and Andersson, 2004). Additionally, the relevance of murine models to *in vivo* human adipose tissue function is minimal as discrepancies between human and mouse data occur (Bouillon et al., 2014). The use of primary cell suspension cultures as well as ceiling cultures have also been used, but are not ideal candidates. The suspension cells lyse within 72 hours of incubation. While ceiling cultures do display lipogenesis and lipolysis, they induce a fibroblast-like phenotype instead of a round adipocyte (Zhang et al., 2000; Sugihara et al., 1986).

Another method in adipose tissue engineering gaining popularity is the differentiation of human adipose-derived stem cells (hASCs) into adipocytes in both two dimensional and three dimensional constructs (Kang et al., 2009; Bellas et al., 2013). These methods have also adopted co-cultures with endothelial cells as an attempt to become more physiologically relevant (Kang et al., 2009; Bellas et al., 2013). These systems are a step in the right direction, but require more time (to differentiate the cells) and contain multilocular lipid droplets rather than unilocular (Gerlach et al., 2012).

In the best-case scenario, explants of human adipose tissue would be cultured on their own. However, this option is not viable as the explanted tissue is delicate and cannot be consistently cultured for longer than fourteen days (Abbott et al., 2016). It was hypothesized that collagen gels could be the answer to the structural integrity problems of culturing the explants, but only the preadipocytes on the edge of the tissue fragments were able to develop actively (Toda et al., 2009).

In this study, an adipose tissue model using a silk sponge scaffold combined with liquefied adipose tissue was utilized. The liquefied lipoaspirate contained a heterogeneous mixture containing of the relevant cell types of adipose tissue: unilocular adipocytes, stromal cells, and endothelial cells. The silk sponge scaffold provides an ECM in which the cells can infiltrate further than collagen gels and provides the structural integrity that allows for long term culture (Abbott et al., 2016).

1.8.1. Efforts to Model Obesity

A variety of approaches have been attempted to stimulate an inflammatory response in an assortment of *in vitro* adipose models (**Table 2**). One strategy determined that exposure to inflammatory cytokine TNF-α stimulates increased rates of lipolysis in differentiated human preadipocytes in a 2D monolayer (Zhang et al., 2002). A separate study found that exposure to different fatty acids (specifically palmitic acid) increased production of TNF-α in 2D monolayers of murine 3T3-L1 adipocytes (Bradley et al., 2008). Another study utilizing 3T3-L1 cells induced the insulin resistance seen in obesity by exposing cells to a variety of materials and conditions: TNF-α, hypoxia, dexamethasone, insulin in high glucose medium, and palmitate (Lo et al., 2013). A 3D 3T3-L1 adipocyte spheroid model modeled the effects of exposure to elevated fatty acid levels followed by acute TNF-α exposure and demonstrated enhanced lipolysis and

decreased metabolic function within cells (Turner et al., 2015). A 3D model using superposition of many sheets of adipocytes differentiated from hASCs demonstrated an increase in MCP-1 when exposed to TNF-α (Aubin et al., 2015). Work using the the 3D silk porous scaffolds soaked in liquefied adipose tissue demonstrated increased insulin stimulated glucose uptake (Abbott et al., Submitted). Most relevant to this work, one study established a co-culture of THP-1 macrophages with differentiated human Simpson-Golabi-Behmel syndrome (SGBS) adipocytes in a 2D monolayer and demonstrated dose-dependent inhibition of adipogenic differentiation and adipocyte apoptosis (Keuper et al., 2011).

Table 2. Summary of various approaches to induce to the inflammatory state of obesity *in vitro.*

Cell Type	*Structure/Dimensionality*	*Stimulus*	*Response*	*Group*
Differentiated human preadipocytes	2D monolayer	TNF-α	Increased lipolysis	Zhang et al. (2002)
Murine 3T3-L1 adipocytes	2D monolayer	Fatty acids	Increased TNF-α production	Bradley et al. (2008)
Murine 3T3-L1 adipocytes	2D monolayer	TNF-α, hypoxia, dexamethasone, insulin in high glucose, palmitate	Insulin resistance	Lo et al. (2013)
Murine 3T3-L1 adipocytes	3D spheroids	Fatty acids, followed by acute TNF-α stimulation	Enhanced lipolysis and decreased metabolic function	Turner et al. (2015)
Differentiated hASCs	3D superpositioned cell sheets	TNF-α	Increased MCP-1 production	Aubin et al. (2015)
Human heterogenous adipose sample	3D silk porous scaffold	TNF-α	Increased glucose uptake in response to insulin and increased lipid droplet size	Abbott et al. (Submitted)
Human SGBS/THP-1 co-culture	2D monolayer	Addition of THP-1 macrophages	Adipocyte apoptosis and inhibition of adipogenic differentiation	Keuper et al. (2011)

1.9. Coherent anti-Stokes Raman Scattering (CARS) Microscopy

In an effort to reduce the use of harmful labeling techniques in imaging, different methods and technologies have been developed. One of these methods is coherent anti-Stokes

Raman scattering (CARS) microscopy. CARS microscopy is one type of coherent Raman microscopy, a way of using coherent excitation of molecular vibrations to generate contrast (Daemen et al., 2016). CARS occurs when a target molecule is irradiated using two short-pulse laser beams, a pump beam and a Stokes beam (**Figure 7**). The frequencies of these two beams must both be tuned such that the difference of their frequencies corresponds to the vibration of the molecule in question. When this is achieved, coherently vibrating molecules in the focal point of the pump and Stokes beams will scatter the probe beam creating a coherent signal with a higher frequency than that of the probe beam and a much larger intensity than the signal from spontaneous Raman scattering (Pezacki et al., 2011).

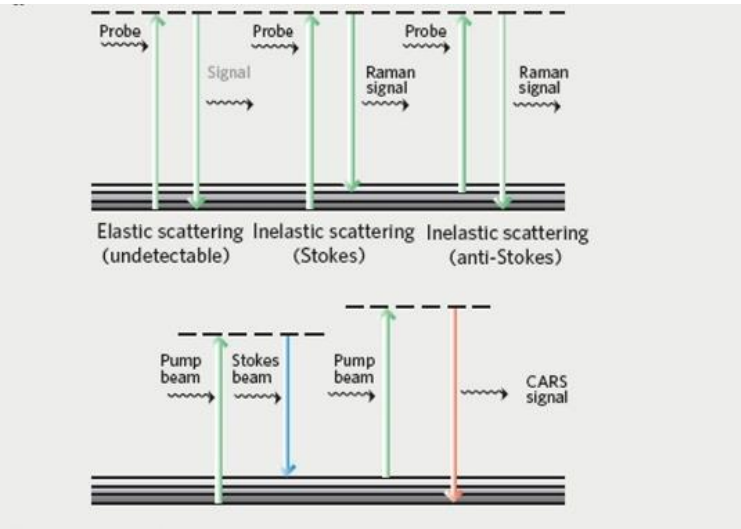

Figure 7. Theory behind CARS microscopy. The schematic highlights the differences between Raman spectroscopy (top) and CARS (bottom) and the need for both a Pump and Stokes beam in CARS spectroscopy (Pezacki et al, 2011).

Lipids have characteristic chemical compositions that distinguish them among other molecules under CARS microscopy. CARS microscopy eliminates the necessity for dyes and allows for real-time, label-free imaging of lipids in samples near physiological conditions. The elimination of fluorescent dyes removes any sources of photobleaching and phototoxicity in samples, which, in turn, allows the samples to be imaged over longer periods of time (Daemen et

al., 2016). The ability to implement real-time imaging in near physiological conditions allows the user to attain different time points without the need for extra samples.

2. Rational Project Design

2.1 Motivation and Problem Statement

As previously mentioned, obesity is a worldwide epidemic. In the United States alone, over a third of adults and over a sixth of children are considered obese. Obesity is not only a domestic problem; since 1980, worldwide obesity has more than doubled with an estimated 600 million obese adults in 2014 (World Health Organization, 2016). Obesity is associated with a variety of health problems such as type 2 diabetes, cardiovascular disease, hypertension, and increased mortality rate me (Kopelmann, 2007). The impact can be felt beyond these individual problems: in the United States, obesity generates annual costs of over $215 billion with no evidence of a decline (Hammond and Levine, 2010).

Obesity is characterized by a state of chronic, low-grade inflammation distinguished by progressive immune cell infiltration into adipose tissues (Bai and Sun, 2015). In an effort to challenge the obesity epidemic, it will be crucial to mimic the state of inflammation in an *in vitro* adipose model. The overall objective of this work was to induce an inflammatory state in an *in vitro* three-dimensional adipose model. To achieve this end, two approaches to induce inflammation were attempted. First, the infiltration of immune cells demonstrated in obesity was simulated by the addition of THP-1 macrophages to the adipose constructs to mimic the low-grade, chronic inflammation seen in obesity. Second, the adipose constructs were exposed to lipopolysaccharide, a known inflammatory stimulant, to induce an acute inflammatory response.

2.2 Hypothesis

The hypothesis of this work is that the simulation of immune cell infiltration will induce an inflammatory state mimicking that of obesity, determined by increased lipolysis and leptin

secretion. It is hypothesized that the M1-polarized macrophages will induce the greatest effect as they are identified by increased production of proinflammatory cytokines. It is hypothesized that the simulation of an acute inflammatory response will produce a more pronounced immediate response while the immune cell infiltration simulation will provide a more delayed, chronic response.

2.3 Aim 1: Confirm THP-1 monocytes can be differentiated into macrophages and polarized towards M1 and M2 states

Being able to use the THP-1 monocytic cell line rather than primary macrophages simplifies experimentation immensely as primary macrophages cannot be expanded ex vivo and have a very limited lifespan. Before using the cell line in experimentation, it was crucial to confirm the ability to differentiate the THP-1 monocytes into a macrophage phenotype and to be able to further polarize them towards M1 and M2 states.

To this end, THP-1 monocytes were exposed to phorbol 12-myristate 13-acetate (PMA) to differentiate them into macrophages (**Figure 8**). Successful differentiation was readily distinguished by cell adhesion to tissue culture plastic and cell spreading. Further, to polarize the cells toward M1 and M2 states, the cells were exposed to interferon gamma (IFNγ) and lipopolysaccharide (LPS) or interleukin 4 (IL-4) and interleukin 13 (IL-13), respectively. Differentiation and polarization were assessed using imaging and gene expression.

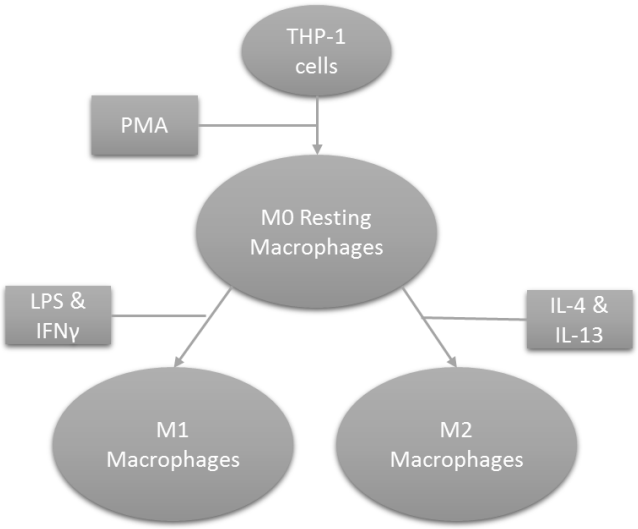

Figure 8. Schematic summarizing the differentiation and polarization process described in Aim 1.

2.4. Aim 2: Simulate the immune cell infiltration seen in obesity in adipose constructs

The goal of this aim was to successfully simulate the immune cell infiltration seen in obesity to mimic its inflammatory environment. The THP-1 macrophages characterized in Aim 1 were utilized as the infiltrating immune cells. Tissue-engineered adipose constructs were seeded with the THP-1 macrophages (**Figure 9**). Three experimental groups will be assessed: seeding of M0 resting macrophages, M1 polarized macrophages, and M2 polarized macrophages. As macrophages have limited lifespan in culture, the THP-1 macrophages were seeded weekly. At various timepoints, the experimental groups and a control group with no added macrophages were assessed to determine lipolysis rates (glycerol secretion), leptin secretion, triglyceride content, DNA content, and protein expression by immunostaining.

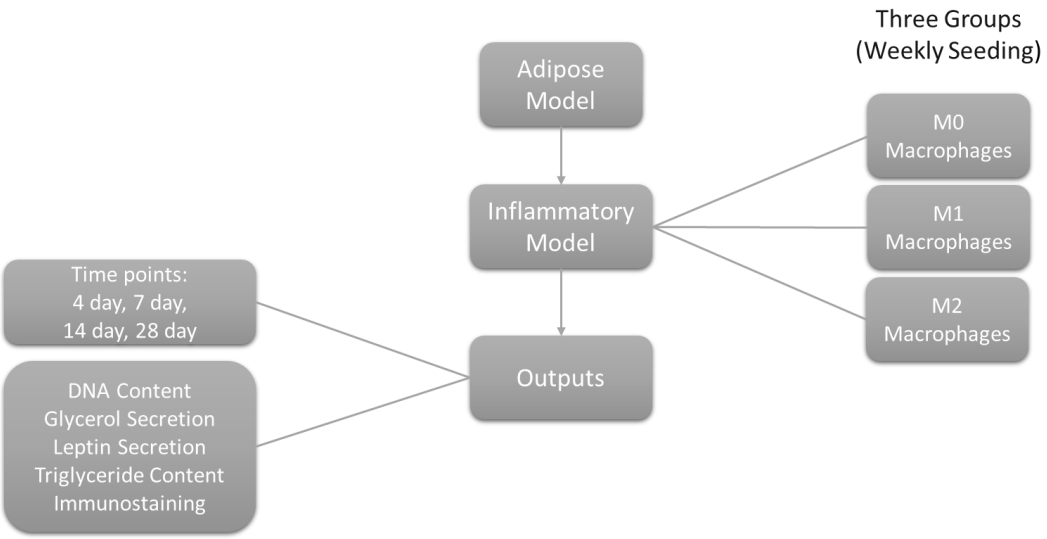

Figure 9. Schematic summarizing the experimental design of the simulated immune cell infiltration described in Aim 2.

2.5. Aim 3: Induce an acute inflammatory response in adipose constructs

The goal of this aim was to determine whether that the adipose constructs could recapitulate an acute inflammatory response (as opposed to the chronic response tested in Aim 2). To this end, the adipose constructs were exposed to lipopolysaccharide (LPS) (**Figure 10**). As LPS is an active component of gram-negative bacterial cell walls that activate acute inflammatory responses, exposure has been shown to upregulate secretion of proinflammatory cytokines. The adipose constructs were exposed to LPS at two different concentrations: the "low" concentration of 1 μg/ml and the "high" concentration of 50 μg/ml. These two experimental groups and a control group were assessed based on lipolysis rates (glycerol secretion) and DNA content.

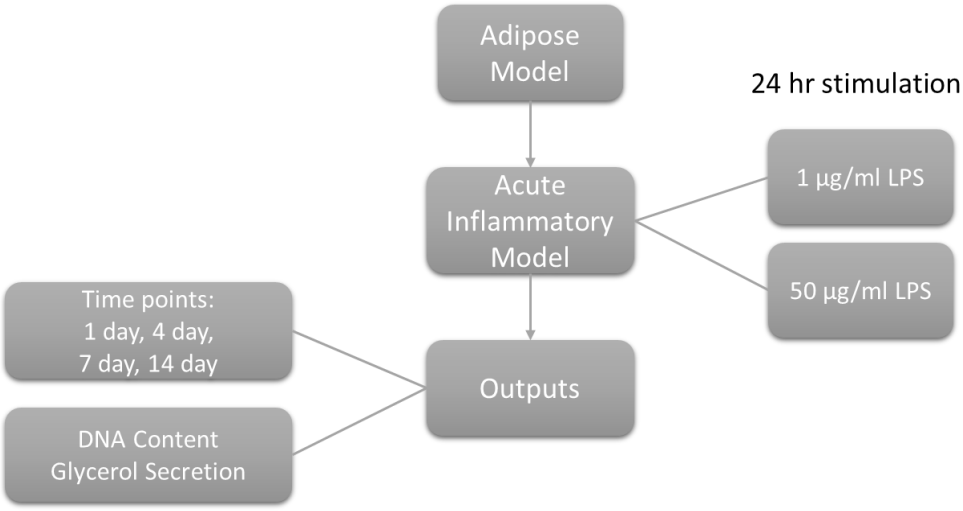

Figure 10. Schematic summarizing the experimental design of acute inflammation stimulation described in Aim 3.

2.6. Innovation

It has been well documented that obese subjects have an increased accumulation of macrophages in their adipose tissue. Moreover, the presence of these macrophages promotes further recruitment of more macrophages. However, there has been little work attempting to simulate immune cell infiltration in an *in vitro* adipose tissue model, and the work that has been done was restricted to two dimensions. Therefore, this work tests the feasibility of co-culturing immune cells with a three-dimensional, physiologically relevant adipose construct to mimic *in vivo* conditions. The tissue engineered adipose construct utilizes a silk fibroin sponge scaffold and hosts the variety of cell types seen in adipose tissue.

The work also provides new information describing the acute inflammatory effects of LPS. LPS has been used as an inflammatory stimulant in a variety of studies both *in vitro* and *in vivo*, but no work has shown its effects on adipose tissue. The adipose construct provides the means to assess LPS as inflammatory stimulant in adipose tissue.

3. Materials and Methods

3.1. Materials List

3.1.1. Cell Culture Materials

ATCC: THP-1 Cell Line cells (#TIB-202) **Peprotech:** Recombinant Human IFN-γ (#300-02), Recombinant Human IL-4 (#200-04), Recombinant Human IL-13(#200-13) **Sigma-Aldrich:** Lipopolysaccharides from Escherichia coli 0111:B4 (#L3012-5MG), 2-Mercaptoethanol (#M6250-100ML), Phorbol 12-myristate 13-acetate (#P8139-5MG)) **ThermoFisher Scientific:** Antibiotic-antimycotic (#15240-062), DMEM/F12 (#11320033), DPBS (#14190250), Fetal bovine serum (#10437-028), HEPES (#15630080), Penicillin-Streptomycin (#15140-122), RPMI 1640 (#11875093), Sodium Pyruvate (#11360070), Trypsin-EDTA (0.25%) phenol red (#25200072)

3.1.2. Assay Materials

Abcam: Anti-CD68 antibody [KP1] (#ab955) **Applied Biosystems**: Power SYBR® Green PCR Master Mix (#4368706) **Bioassay Systems:** EnzyChrom Adipolysis Assay Kit (#EAPL-200), EnzyChrom Triglyceride Assay Kit (#ETGA-200) **Biorad**: iScript™ Advanced cDNA Synthesis Kit for RT-qPCR (#1725038) **Qiagen:** QIAshredder (#79656), RNeasy Mini Kit (#74104) **ThermoFisher Scientific:** DAPI (#D1306),10% Normal Goat Serum (#50062Z), Primers (see Table x), Quant-iT™ PicoGreen® dsDNA Assay Kit (#P11496) **Sigma-Aldrich**: Anti-Mouse IgG (whole molecule)–FITC antibody produced in goat (#F0257-1ML), Human Leptin ELISA Kit (#RAB0333-1KT)

3.1.3. Other Materials

Chinese Collaborator: *Bombyx mori* Cocoons **Sigma Aldrich:** 1,1,1,3,3,3-Hexafluoro-2-Propanol (HFIP) (#105228), Sodium Chloride (NaCl, ASC reagent) (#S9888) **ThermoFisher:** 4 mm biopsy punches (#NC9840633)

Table 3. List of primers used for RT-qPCR

Gene of Interest	Forward Sequence	Reverse Sequence
GAPDH	TTCGACAGTCAGCCGCATCTTCTT	ACCAAATCCGTTGACTCCGACCTT
TNF-α	CTGCTGCACTTTGGAGTGAT	AGATGATCTGACTGCCTGGG
MRC-1	CAGCGCTTGTGATCTTCATT	TACCCCTGCTCCTGGTTTTT
IL-6	AGCCACTCACCTCTTCAGAAC	GCCTCTTTGCTGCTTTCACAC

3.2. THP-1 Differentiation and Polarization Study

To simulate the infiltration of macrophages, a source of macrophages was necessary. The THP-1 monocytic cell line (ATCC) was chosen as a potential source. THP-1 cells were maintained in RPMI 1640 supplemented with fetal bovine serum (10% v/v), HEPES (10 mM), sodium pyruvate (1 mM), 2-Mercaptoethanol (0.05 mM), and penicillin streptomycin (1% v/v) (referred to hereafter as THP-1 Media) in T 75 cm^2 tissue culture flasks in a humidified incubator (37° C/ 5% CO_2) (Lund et al., 2016; Tulk et al., 2015). Cells were expanded to obtain sufficient cell densities.

To differentiate the THP-1 cells towards a macrophage phenotype, THP-1 cells (2 x 10^5 cells/ml) were incubated with phorbol 12-myristate 13-acetate (PMA, 25nM) diluted in THP-1 Media in 24-well tissue culture plates for 48 h. After the 48-h differentiation period, the PMA containing media was removed, the cells were rinsed with phosphate buffered saline (PBS), and

then replaced with THP-1 Media for a 24-h recovery period. After this recovery period, the THP-1 cells were differentiated into M0 resting macrophages (Lund et al., 2016). To polarize the M0 macrophages towards M1 and M2 activated states, the cells were incubated with THP-1 Media supplemented with lipopolysaccharide (LPS, 1µg/ml) and interferon gamma (IFN-γ, 20 ng/ml) or interleukin 4 (IL-4, 20 ng/ml) and interleukin 13 (IL-13, 20 ng/ml) for 24 h, respectively (Chanput et al., 2013; Genin et al., 2015). To assess differentiation and polarization, samples were taken for both RT-qPCR as well as fixed in 10% neutral buffered formalin for immunohistochemistry.

3.3. Silk Processing

In order to use silk as a biomaterial, the silk fibroin protein had to first be purified (**Figure 11**). *Bombyx mori* silk cocoons were used as the source of silk fibroin as described previously (Rockwood et al., 2011). The cocoons were cut into dime-size pieces, and the worms were taken out. Cocoon pieces were then boiled for 30 min, where every 5 grams of cocoon were boiled with 2 L of water and 4.24 gram of sodium bicarbonate (0.02 M sodium bicarbonate solution). The resulting fibers were then rinsed in milliQ water for 20 minutes three separate times. Excess water was then squeezed out, and the fibers were allowed to dry overnight. The silk fibers were then dissolved in 9.3 M lithium bromide (LiBr) (20% w/v) and incubated at 60 °C for 4 hours. The silk/LiBr solution was then added to dialysis cassettes and dialyzed against ultrapure water for 3 days. During those 3 days, the water was changed a total of 6 times: 3 changes on the first day, 2 changes on the second day, and 1 change on the last day. The silk solution was then removed from the cassette, centrifuged twice at 9000 rpm to remove remaining debris, and then frozen and stored at -20 °C (Rockwood et al., 2011).

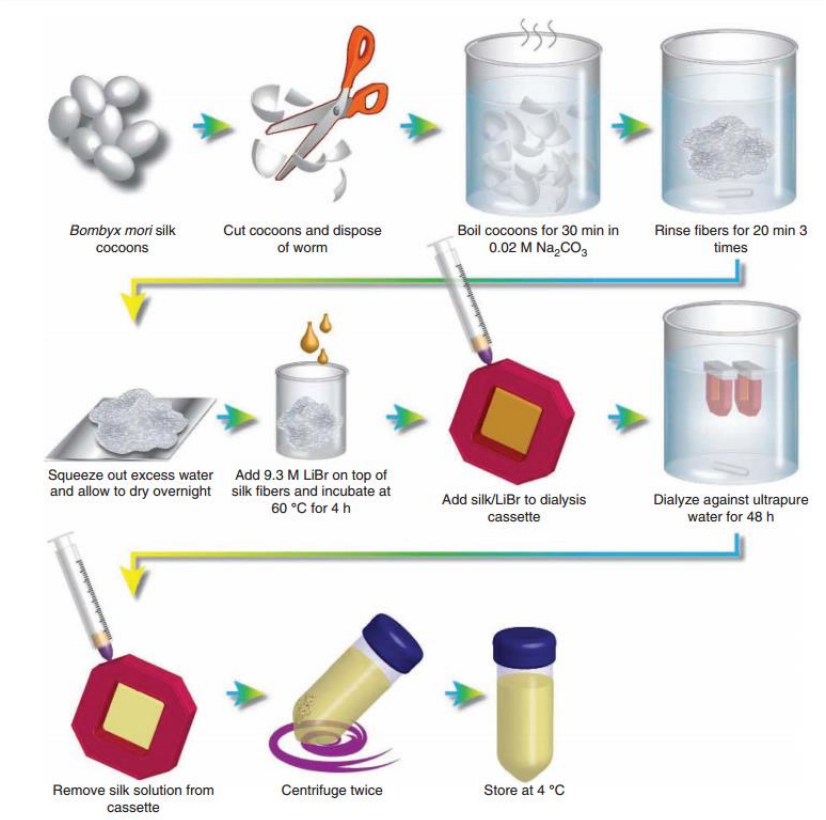

Figure 11. Schematic illustrating the process of attaining an aqueous silk fibroin solution from *Bombyx mori* silk cocoons (Rockwood et al., 2011).

3.4. Silk Scaffold Preparation

Porous silk sponge scaffolds are used to support adipose tissue growth as they allow for adequate transfer of nutrients and are relatively soft to mimic the modulus of adipose tissue. In order to prepare the silk sponges, the following protocol was used (**Figure 12**). The frozen silk solution was placed in a lyophilizer for 2 days to remove all water from the silk. Once lyophilized, every 1.7 grams of silk were dissolved in 9 ml of helafluoro-2-propanol (HFIP) to create a 17% (w/v) silk-HFIP solution. Sieved sodium chloride (NaCl) crystals (500-600 μm grain size) were used as porogens to create the appropriate sized pores for the silk sponge scaffold. 2 mL of the 17% silk-HFIP solution were added over 6.8 grams of the NaCl in 20mm

diameter polyethylene capsules with a syringe. The caps of the capsules were closed, and the capsules were left in a fume hood for 2 days to allow for even distribution of the silk/HFIP solution within the salt. After 2 days, the capsules were then opened and left in the fume hood overnight to allow for the HFIP to evaporate. The capsules were then placed in methanol overnight to form β-sheets and increase stability of the structure. They were then removed from the methanol and placed in a fume hood overnight to allow any residual methanol to evaporate. The capsules were then immersed in milliQ water to leach out the NaCl leaving behind empty pores. Once the salt was removed from the scaffolds (indicated by the scaffolds floating in water), the scaffolds were cut to the desired size cylinder (2mm height x 4mm diameter) using a PDMS mold, razor blade, and 4 mm biopsy punch.

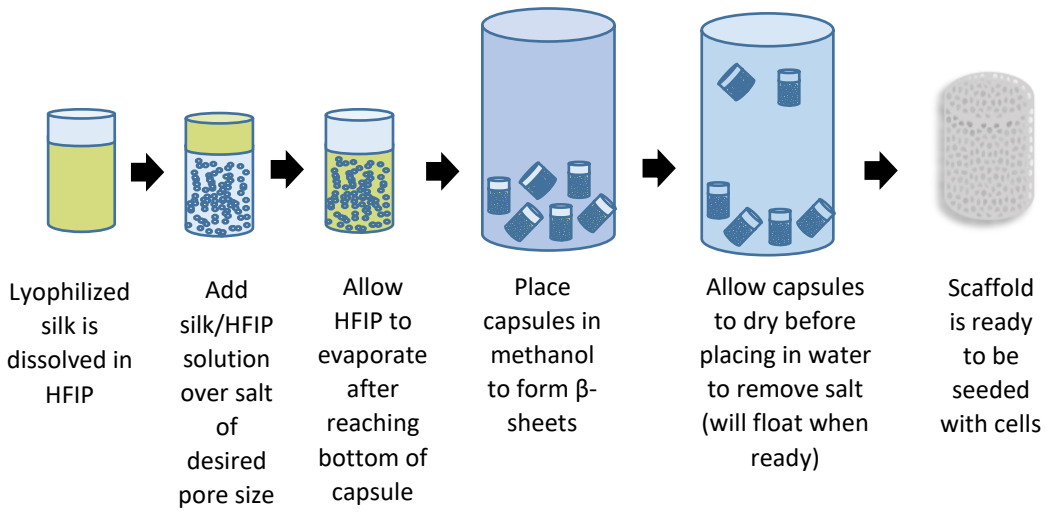

Figure 12. Schematic illustrating the process of fabricating silk sponge scaffolds from lyophilized silk solution.

3.5. Primary Lipoaspirate Isolation and Cell Seeding

To prepare the cut scaffolds for cell seeding, scaffolds were autoclaved to sterilize the scaffold and were then soaked in DMEM/F12 supplemented with fetal bovine serum (10 % v/v), and Antibiotic-Antimycotic (1% v/v) (referred to hereafter as Maintenance Media).

On the same day of surgery, subcutaneous adipose tissue was acquired from elective abdominoplasty procedures. Blunt dissection was used to separate the adipose tissue from the skin and the fascia of Scarpa. The adipose tissue was liquefied in a blender by successive short pulses until the tissue had the viscosity of lipoaspirate. Media was then aspirated from the soaking scaffolds, and the scaffolds were added directly to the liquefied adipose tissue in 50 mL falcon tubes. The tubes were placed in an incubator for 1 h (37 °C, 5% CO2). The scaffolds were then separated from the excess tissue and placed into 24 well plates for 2 h (37 °C, 5% CO2) without media to allow the cells to attach to the scaffold. Maintenance Media was then added and changed twice a week until the constructs were ready to be used (Abbott et al., 2016). **Table 4** describes known information of the adipose sample used in these studies.

Table 4. Known information on patient samples used. All patients were non-diabetics.

Patient	*Age*	*Sex*	*BMI*
1	58	Male	39
2	71	Female	24.3
3	40	Female	35.1
4	63	Female	74.2

3.6. Macrophage Infiltration Study

About a week after the seeding of scaffolds, the THP1 macrophages were added dropwise to the constructs (175,000 cells/constructs) in the four experimental groups of Control, M0 macrophages, M1 macrophages, and M2 macrophages. The THP-1 macrophages were grown, differentiated, and polarized as previously described (**Section 3.2**) in T 75 cm^2 tissue culture flasks. On the day of seeding, macrophages were detached from the tissue culture flasks by incubating with Trypsin-EDTA and counted using a hemocytometer before the constructs were seeded. The various rounds of experiments each used an adipose sample from a different patient and ranged from 7 days to 28 days with timepoints taken at Day 0, 4, 7, 14, and 28 (cell lysis and supernatants). Macrophages were seeded onto the constructs weekly. Maintenance Media was changed twice per week.

3.7. LPS Acute Inflammation Study

About a week after the seeding of scaffolds, the adipose constructs were exposed to varying levels of LPS for 24 h in the three experimental groups of Control (no LPS), 1 μg/ml LPS, and 50 μg/ml LPS. The constructs were then cultured for 14 days with timepoints taken at Day 0, 1, 4, 7, and 14 (cell lysis and supernatants). Maintenance Media was changed twice per week.

3.8 Assays

3.8.1. RT-qPCR

Each sample for RT-qPCR was kept in 300 μL of RLT buffer, 3 μL of 2-mercaptoethanol, and 0.43 μL of RNA carrier. Samples were frozen at -80°C until used.

3.8.1.1. RNA Isolation

This method was adapted from the Qiagen RNeasy® Mini Kit, Part 1 protocol. First, RNAse Zap was sprayed on the work surfaces to prevent any contamination of samples. The samples were thawed from -80°C, added to QIAshredder cell-lysate homogenizers and centrifuged at maximum speed for 3 minutes. The leftover supernatants were taken and each sample was combined with equal parts of 70% ethanol. 700 µL of sample and ethanol mixture was transferred to an RNeasy mini spin column and centrifuged at 8000 g for 15 seconds. The flow through was disposed of and 700 µL of Buffer RW1 was added to the spin column. The samples were centrifuged at 8000 g for 15 seconds and the flow through was again disposed of. Next, 500 µL of Buffer RPE was added to the spin column, the samples were again centrifuged at 8000 g for 15 seconds, and the flow through was discarded. This step was done twice, centrifuging for 2 minutes the second time to ensure that the samples were washed cleanly. The spin columns were placed in a new 1.5 mL collection tube and 50 µL of RNase-free water was added to the spin column membrane. The samples were centrifuged for 1 minute at 8000 g to elute the isolated RNA.

3.8.1.2. NanoDrop

The NanoDrop roughly estimated how much nucleic acid was in the sample. The NanoDrop was blanked with DI water as a control, and 1 µL of each sample was tested for nucleic acid concentration. The RNA was then stored at -80°C.

3.8.1.3. cDNA Synthesis

This method is adapted from iScript™ Advanced cDNA Synthesis Kit for RT-qPCR protocol.

The RNA samples were first thawed from -80°C and were transferred into PCR tube strips. 4 µL of 5x iScript Advanced Reaction Mix and 1 µL of iScript Advance Reverse Transcriptase for every 15 µL of sample were added to each tube, and the strips were placed in a thermal cycler at the following settings: 20 minutes at 46°C for reverse transcription to occur and 1 minute at 95°C to inactivate the reverse transcription. The samples were then taken out of the thermal cycler and stored in -20°C until use.

3.8.1.4. RT-qPCR

The cDNA samples were thawed from -20°C. For each gene of interest, each sample was run in triplicate. For each reaction, 9.2 µL of cDNA (diluted with DNase and RNase free water) was added to the PCR plate combined with 0.4 µL of forward primer, 0.4 µL of reverse primer, and 10 µL of Power SYBR® Green PCR Master Mix (list of primers can be found in **Table 3**). The thermal profile setup of the RT-qPCR reaction was as follows: 1. 10 min at 95°C for one cycle 2. 30 seconds at 95°C, 1 minute at 58°C, and 1 minute at 72°C for 40 cycles 3. 30 seconds at 95°C, 30 seconds at 58°C, and 30 seconds at 95°C for 1 cycle.

3.8.2. Picogreen DNA Quantification Assay

This method is adapted from Invitrogen Picogreen Assay Kit protocol. First, the cell samples were thawed from -20°C. The cells were kept in 1x TE buffer that solubilized the cell membranes leaving a cell lysis. 25 µL of sample lysis and 75 µL of 1x TE buffer were added to each well of a 96-well plate in duplicate. Standards were made using the standard supplied in the kit and 1x TE buffer. 100 µL of 2µg/ml dye (diluted with 1x TE buffer) was added to each well

and the fluorescence was immediately measured on a plate reader at an excitation of 480 nm and an emission of 520 nm.

3.8.3. Glycerol Secretion Quantification Assay

This method is adapted from Bioassay Systems EnzyChrom Adipolysis Assay Kit protocol. First, the cell culture supernatant samples were thawed from -20°C. 10 µL of each sample was pipetted into a well on a 96-well plate in duplicate. A working reagent combining the reagents supplied in the kit was made with 100 µL of assay buffer, 2 µL of enzyme mix, 1µL of ATP, and 1µL of dye reagent for each well. 100 µL of working reagent was then pipetted into each well and the plate was incubated for 20 minutes at room temperature. After incubation, the optical density was measured on a plate reader at 570 nm.

3.8.4. Leptin Secretion Enzyme-Linked Immunosorbent Assay (ELISA)

This method is adapted from the Sigma-Aldrich Human Leptin ELISA Kit protocol (**Figure 13**). First, all cell supernatant samples and reagents were thawed from -20°C. 100 µL of sample and standard were added to the Human Leptin Antibody-coated ELISA plate and incubated for 2.5 hours. Following this incubation, the plate was washed four times with 1x Wash Solution and then 100 µL of Biotinylated Human Leptin Detection Antibody was added to the plate and incubated for one hour. Following this second incubation, the plate was again washed four times with the 1x Wash Solution. Following the wash, 100 µL of 1x HRP-Streptavidin solution was added to the plate and incubated for forty-five minutes. Following this third incubation, the final four-time wash with 1X Wash Solution was completed followed by the addition 100 µL of the Colorimetric TMB Substrate Reagent. The plate was than incubated in the dark and periodically

checked until the most concentrated standard approached saturation. At that time, 50 µL of Stop Solution was added to the plate before reading the optical density on a plate reader at 450 nm. All incubations were at room temperature with gentle shaking.

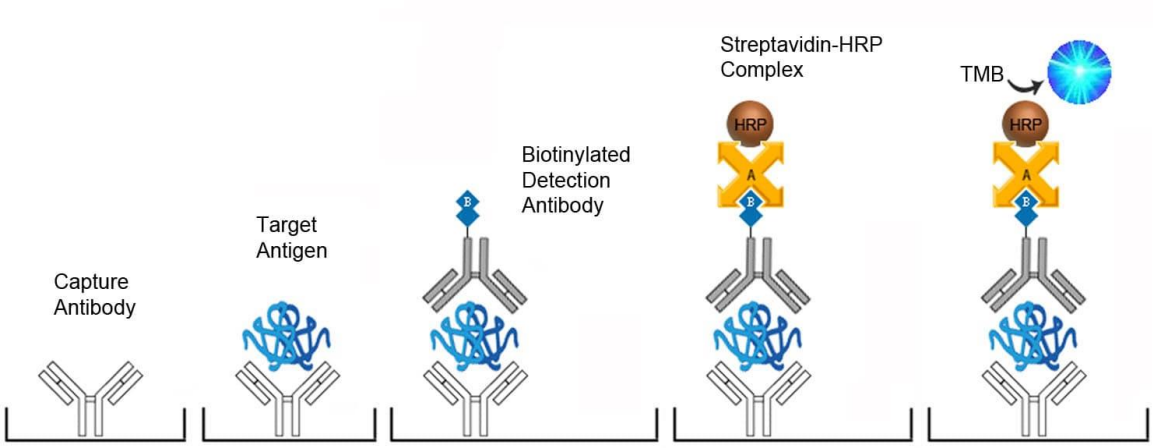

Figure 13. Schematic describing the sandwich ELISA process (LifeSpan BioSciences, Inc.)

3.8.5. Intracellular Triglyceride Quantification Assay

This method is adapted from Bioassay Systems EnzyChrom Triglyceride Assay Kit protocol. First, the cell samples were thawed from -20°C. The cells were kept in 1x TE buffer solubilizing the cell membranes. Next, 10 µL of each sample was pipetted into a well on a 96 well plate in duplicate. A working reagent combining the reagents supplied in the kit was made, with 100 µL of assay buffer, 2 µL of enzyme mix, 5µL of lipase, 1 µL of ATP, and 1µL of dye reagent for each well. 100 µL of working reagent was then pipetted into each well and the plate was incubated for 30 minutes at room temperature. The optical density was then measured on a plate reader at 570 nm.

3.9. Immunohistochemistry

Scaffold samples were fixed in 10% neutral buffered formalin for one hour to preserve the structure of their proteins through crosslinking. After fixation, samples were washed three times

in PBS and then blocked in buffer (10% goat serum, 1% bovine serum albumin, and 1% triton in PBS) for 1 h to inhibit nonspecific protein-protein interactions and permeabilize the cells. The samples were then incubated with the primary Anti-CD68 (human cluster of differentiation 68) antibody (1:200 in PBS) for one hour at room temperature followed by three 10 min washes of PBS to get rid of any residual primary antibody. The samples were then incubated with the secondary Anti-Mouse IgG (whole molecule)–FITC antibody produced in goat (1:200) and DAPI (1:1000) for one hour at room temperature. This was followed by another set of three 10 min washes in PBS to remove residual primary antibody and DAPI to reduce background noise. The samples were then imaged on the Leica SP8 confocal microscope.

3.10 Statistical Analysis

For the THP-1 polarization study, a 1 way ANOVA was performed for the different polarization methods to analyze the RT-qPCR results. A Dunnett's post hoc test was performed to compare the experimental polarization groups to the non-polarized control. A Tukey's post hoc test was performed to compare the two polarization methods. In the immune cell infiltration simulation study, to analyze DNA content, triglyceride content, leptin secretion, and glycerol secretion, a 2 way ANOVA was performed where the factors were the time cultured and the type of macrophage seeded onto the scaffolds. A Tukey post hoc test was performed for significant factors and interactions. In the acute inflammation study, a 2 way ANOVA was performed where the factors were the time cultured and the concentration of LPS used. A Tukey post hoc test was performed for significant factors and interactions. Significance was always defined as $p<0.05$.

4. Results

4.1. Aim 1. Confirming THP-1 monocytes can be differentiated into macrophages and polarized towards M1 and M2 states

To simulate the infiltration of immune cells seen in obesity, a source of immune cells was needed. It was hypothesized that the THP-1 monocytic cell line could be used, but it was important to confirm that these monocytes could be differentiated into macrophages and further polarized into M1 and M2 states. After applying the differentiation and polarization protocol previously described (**Section 3.2**), the cells were assessed through imaging and gene expression.

4.1.1. Imaging

As THP-1 monocytes are suspension cells, an immediate sign of differentiation was cell adhesion to tissue culture plastic. M1-polarized macrophages typically are more elongated and spread out while M2-polarized macrophages are more rounded. **Figure 14** shows the cells after both differentiation and polarization. All groups became adherent. The M1-polarized cells displayed the elongated morphology and had an increased amount of lipid depots. The M2-polarized cells displayed greater confluency than the other groups and the expected rounded phenotype.

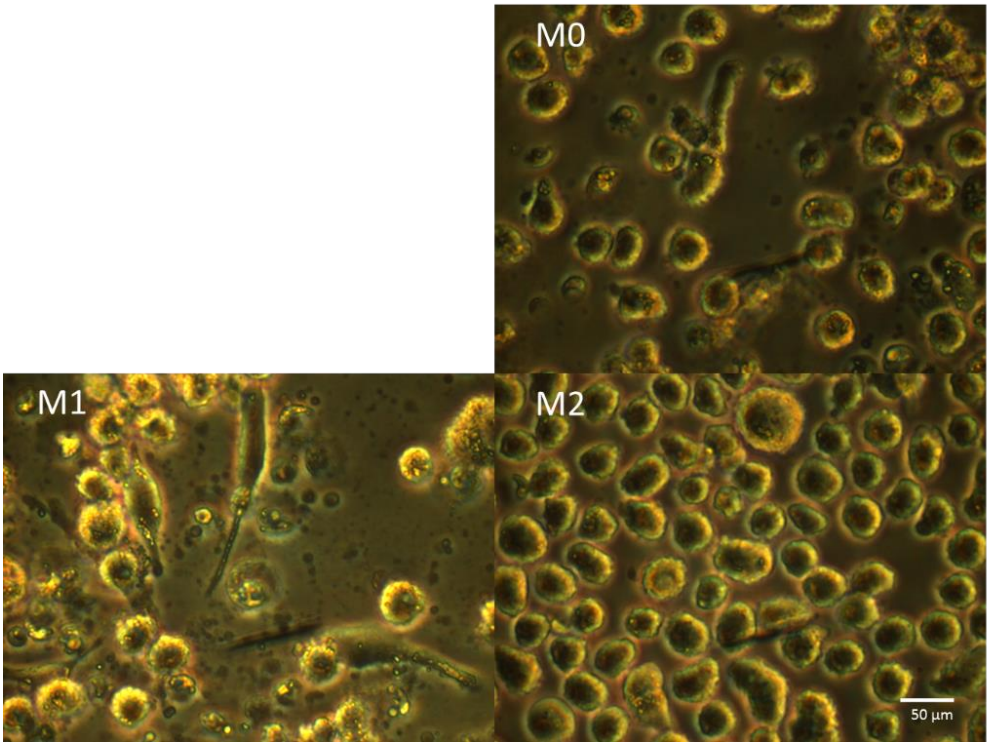

Figure 14. Brightfield images of THP-1 macrophages were taken with a light microscope after the differentiation and polarization process. Representative images of each group (M0 (no polarization), M1 polarization, and M2 polarization) are shown. Scale bar is 50 µm in length.

Fluorescent images (**Figure 15)** further confirmed successful differentiation in macrophages. Using immunohistochemistry, the cells were stained for human cluster of differentiation (CD68), a general macrophage marker. The cells were also stained with DAPI to denote cell nuclei and imaged with coherent anti-Stokes Raman spectroscopy (CARS) to image lipids. All groups displayed CD68 expression, and consistent with the brightfield images, the M1-polarized cells showed an increased accumulation of lipids.

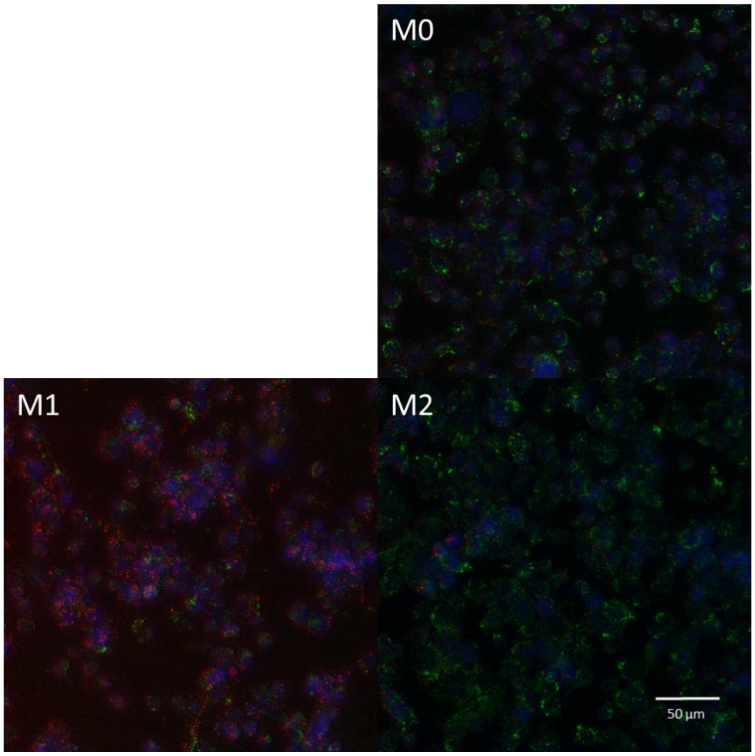

Figure 15. Fluorescent images of the THP-1 macrophages were taken with a confocal microscope after the differentiation and polarization process. Cells were stained with DAPI (blue) to denote cell nuclei and CD68 (green), a macrophage marker. Coherent anti-Stokes Raman spectroscopy was simultaneously used to image the lipids within the cells (red).

4.1.2. Gene Expression

For use as a disease model, it was important to polarize the macrophages towards M1 and M2 phenotypes. To ensure the polarization protocols used were producing these phenotypes, gene expression was assessed. Expression of the M1 markers TNF-α (tumor necrosis factor alpha) and IL-6 (interleukin 6) and the M2 marker MRC-1 (mannose receptor C-type 1) was assessed. The experiment was executed two separate times to ensure reproducibility (**Figure 16A** and **Figure 16B**). Significant upregulation of the M1 marker genes was seen in the M1 polarization group in both cases. Similarly, significant upregulation of the MRC-1 was seen in the M2 polarization group, and the M1 polarization group showed significant downregulation of MRC-1.

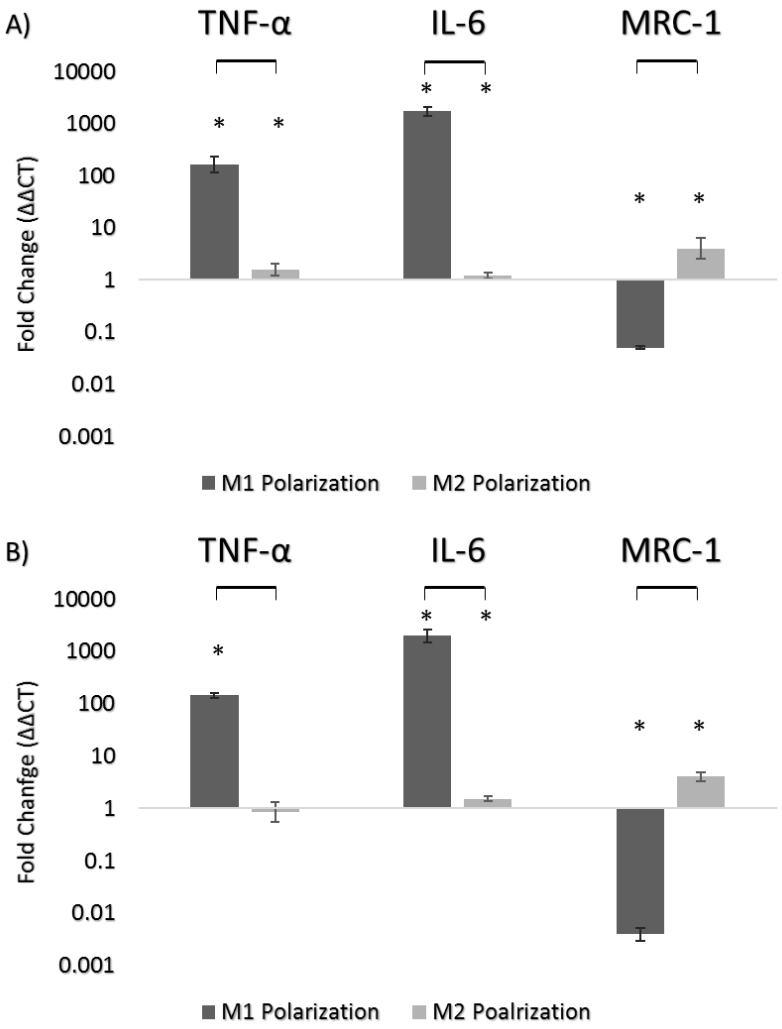

Figure 16. Successful macrophage polarization was determined by gene expression using RT-qPCR. The genes assessed were TNF-α (M1 Marker), IL-6 (M1 marker), and MRC-1 (M2 marker). The polarization experimental groups were both normalized by a housekeeping gene (GAPDH) and compared to a non-polarized M0 control. The experiment was executed twice (A and B). A 1 way ANOVA was performed for the different polarization methods ($p < 0.0001$ for both A and B) A Dunnett's post hoc test was performed to compare the experimental polarization groups to the non-polarized control where significance is denoted by a "*". A Tukey's post hoc test was performed to compare the two polarization methods where significance was denoted with bars between them. Significance was defined as $p < 0.05$. Samples were run in triplicate with at least n=4. Error bars represent standard error of the mean.

4.2. Aim 2: Simulating the immune cell infiltration seen in obesity in adipose constructs

After the THP-1 cell line was determined to be a viable cell source, the simulation of immune cell infiltration was attempted. Three experimental groups were assessed: seeding of M0 resting macrophages, M1 polarized macrophages, and M2 polarized macrophages. A control group with no macrophages was also assessed. Results shown display experiments using adipose samples from three separate patients: Patient 1, Patient 2, and Patient 3 **(Table 4)**, and the culture time of the experiments ranged from 14 to 28 days with samples taken at days 4, 7, 14, and 28, when applicable. Constructs were quantitatively assessed based on DNA content, triglyceride content, leptin secretion, and glycerol secretion. Additionally, confocal imaging was used to qualitatively assess the constructs.

4.2.1. DNA Content

First, DNA content was analyzed to assess how the different culture conditions as well as the time cultured affected cell number in the constructs (**Figure 17)**. The results varied depending on the adipose sample. Constructs using cells from Patient 1 (**Figure 17A)** showed no significant differences between culture conditions within the same timepoints. However, in all cases, DNA content increased with increased culture time. Constructs from Patient 2 (**Figure 17B**) also displayed increased DNA content over time barring the control group. Unlike the first patient, different culture conditions exhibited significant differences after 14 days of culture. At day 14, constructs seeded with M0 macrophages exhibited increased cell proliferation compared to all other groups, and at day 28, constructs seeded with M0 and M2 macrophages displayed increased proliferation compared to the control group and constructs seeded with M1 macrophages. Samples from Patient 3 (**Figure 17C**) displayed similar increases in DNA content

with time. At day 14, only constructs seeded with M2 macrophages displayed a significant increase in DNA content compared to the control, but at day 28, all three experimental groups exhibited a significant increase when compared to the control group.

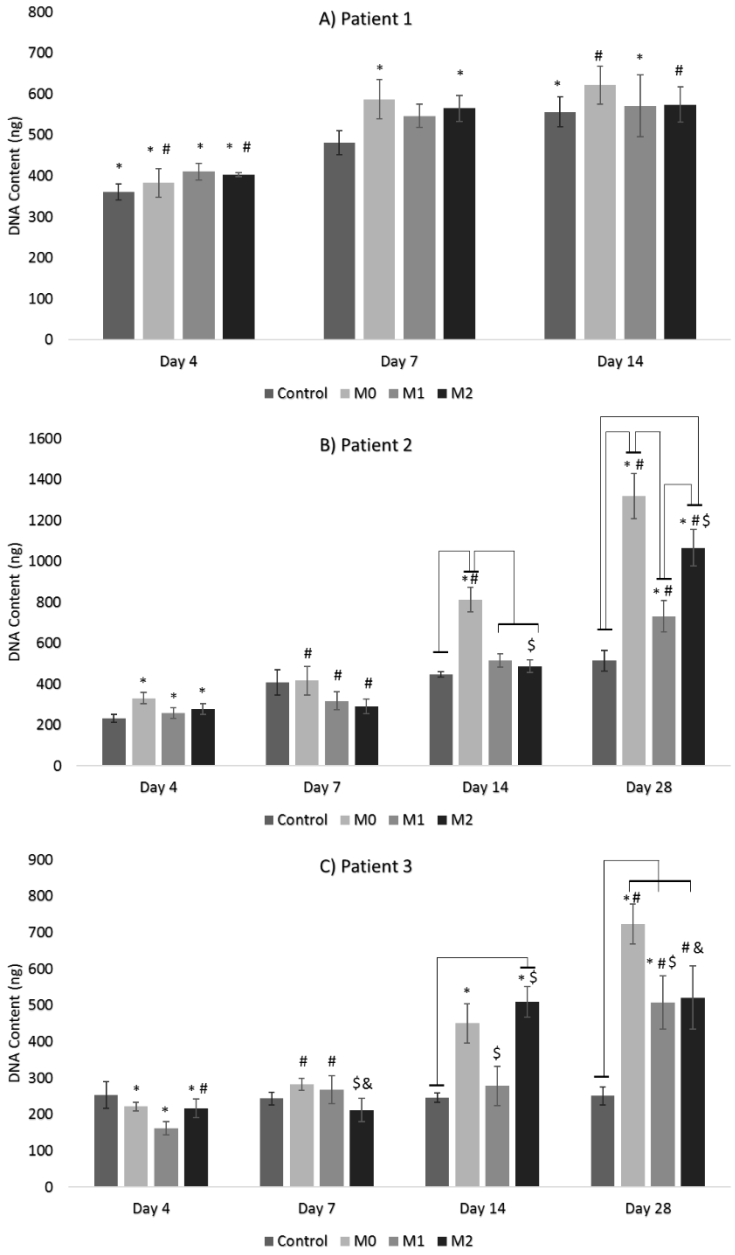

Figure 17. DNA content of the constructs was determined to assess changes in cell number at different timepoints and among different culture conditions. A 2 way ANOVA was performed where the factors were the time cultured and the type of macrophage seeded onto the scaffolds. Constructs using the sample of Patient 1 (**A**) did not display a significant effect of the factors interacting, but did vary over time ($p<0.0001$). Constructs using samples Patients 2 and 3 (**B** and **C)** did display a significant effect of the two factors interacting ($p<0.0001$). A Tukey post hoc test was performed for significant factors and interactions. Significance between macrophage seeding groups within certain timepoints are denoted by lines connecting them. Significance between timepoints within the same macrophage seeding group is denoted by a shared symbol. Significance was defined as $p<0.05$. Samples were run in duplicate with at least $n=4$. Error bars represent standard error of the mean.

4.2.2. Triglyceride Content

Next, triglyceride content was analyzed based on the different culture conditions as well as the time cultured, and it was normalized by the DNA content of constructs (**Figure 18)**. Again, results varied based on the patient. Consistent with DNA content, samples from Patient 1 (**Figure 18A**) varied based on time cultured with no differences between culture conditions. However, the trend was the opposite of DNA content where triglycerides content decreased over time. Patient 2 constructs (**Figure 18B)** and Patient 3 constructs (**Figure 18C)** both showed changes over time and between culture conditions. The trends were inversely dependent on the DNA content that the results were normalized by (**Figure 17).** Typically, where there was increased DNA content, the normalized triglyceride content was decreased.

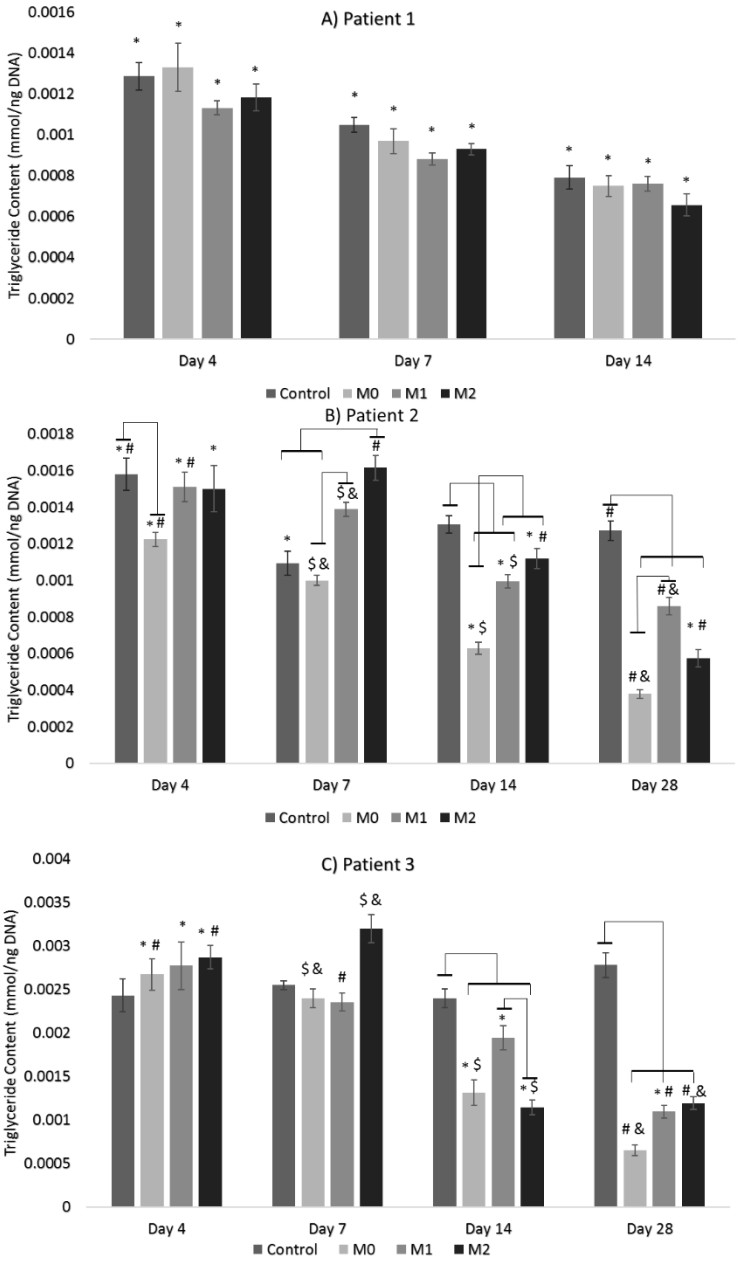

Figure 18. Triglyceride content of the constructs was assessed at different timepoints and among different culture conditions and normalized by DNA content. A 2 way ANOVA was performed where the factors were the time cultured and the type of macrophage seeded onto the scaffolds. Constructs using the sample of Patient 1 (**A**) did not display a significant effect of the factors interacting, but did vary over time ($p<0.0001$). Constructs using samples from Patients 1 and 2 (**B** and **C)** did display a significant effect of the two factors interacting ($p<0.0001$). A Tukey post hoc test was performed for significant factors and interactions. Significance between macrophage seeding groups within certain timepoints are denoted by lines connecting them. Significance between timepoints within the same macrophage seeding group is denoted by a shared symbol. Significance was defined as $p<0.05$. Samples were run in duplicate with at least n=4. Error bars represent standard error of the mean.

4.2.3. Leptin Secretion

Next, leptin secretion was analyzed based on the different culture conditions as well as the time cultured, and it was normalized by the DNA content of the constructs **(Figure 19**). As with previous assessments, the results varied depending on the patient. Comparisons within patient samples displayed differences depending on both time and culture conditions. Constructs from Patient 1 (**Figure 19A**) displayed a decrease in leptin secretion over time in the constructs seeded with M2 macrophages where the other groups exhibited no significant changes over time. At day 4, constructs seeded with M1 and M2 macrophages secreted significantly more leptin than the control group. At Day 14, the constructs seeded with M0 and M1 macrophages secreted more leptin than both the control group and the constructs seeded with M2 macrophages. The second patient (**Figure 19B**) displayed different trends from the first patient. At days 4, 7, and 14, constructs seeded with M0 macrophages showed a significant increase in leptin secretion. However, at day 28, constructs seeded with M0 macrophages showed a significant decrease when compared to the control. Typically, leptin secretion decreased over time among groups. Finally, the third patient (**Figure 19C**) had the greatest overall magnitude of leptin secretion compared to the other patients (similar to the enhanced triglyceride content of this sample). Consistent with the other two patient samples, leptin secretion decreased over time. At day 4, all constructs seeded with macrophages exhibited significantly higher leptin secretion than the control. At days 7 and 14, constructs seeded with M0 and M1 macrophages displayed significantly higher secretions than the other groups, and those seeded with M1 macrophages secreted more leptin than those seeded with M0 macrophages. At day 28, leptin secretion significantly decreased in magnitude in all groups besides those seeded with M2 macrophages which showed increased secretion when compared to its day 14 counterpart. Constructs seeded

both with M1 and M2 macrophages showed significantly higher secretion when compared to the control.

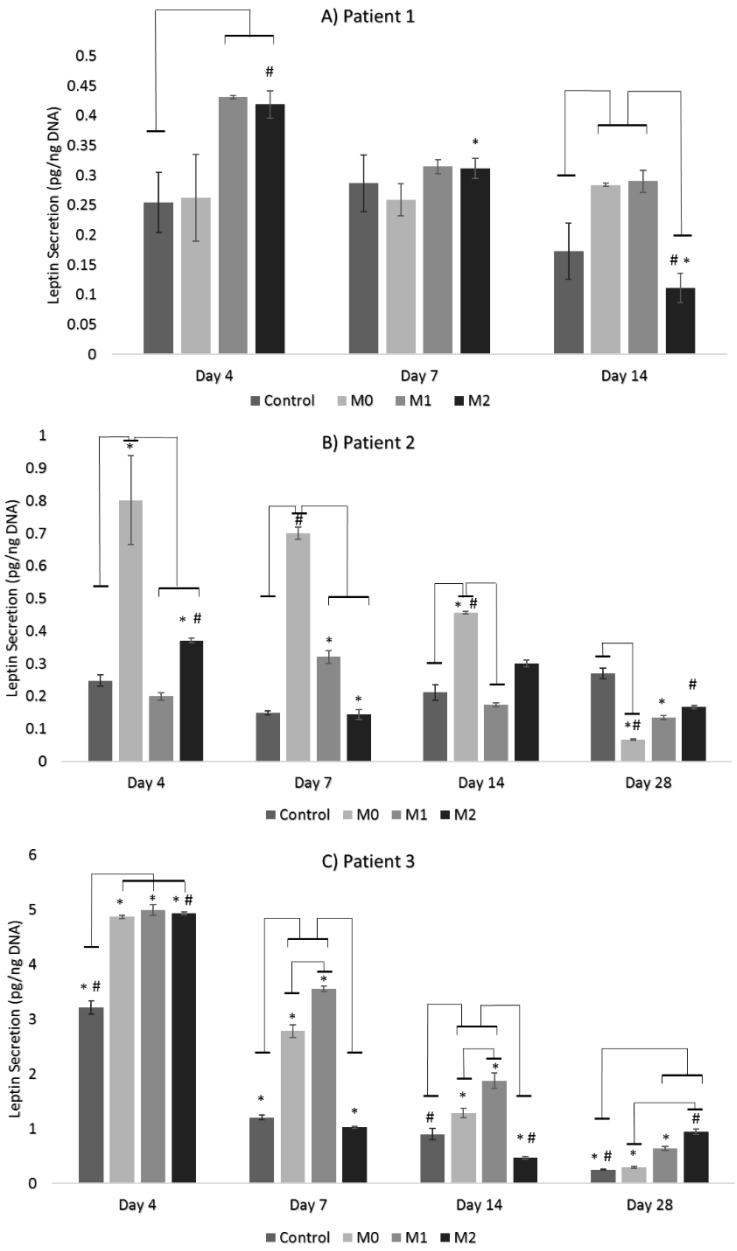

Figure 19. Leptin secretion of the constructs was assessed at different timepoints and among different culture conditions and normalized by DNA content. A 2 way ANOVA was performed where the factors were the time cultured and the type of macrophage seeded onto the scaffolds. Constructs using samples Patients 1, 2, and 3 (**A, B,** and **C)** all displayed a significant effect of the two factors interacting (Patient 1 with $p=0.007$ and others $p<0.0001$). A Tukey post hoc test was performed for significant factors and interactions. Significance between macrophage seeding groups within certain timepoints are denoted by lines connecting them. Significance between timepoints within the same macrophage seeding group is denoted by a shared symbol. Significance was defined as $p<0.05$. Samples were run in duplicate with at least $n=4$. Error bars represent standard error of the mean.

4.2.4. Glycerol Secretion

Next, glycerol secretion was analyzed to assess lipolysis rates based on the different culture conditions as well as the time in culture. Glycerol secretion was normalized by the DNA content of the constructs **(Figure 20**). As with previous assessments, the results varied depending on the patient. Overall, Patient 1 (**Figure 20A)** displayed decreases in glycerol secretion over time. Constructs from the second patient (**Figure 20B)** behaved differently. At days 4, 7, and 14, the constructs seeded with M0 and M1 macrophages showed lower secretion levels than the other groups. However, at Day 28, constructs seeded with M1 macrophages secreted similar levels to those of the other groups, and the constructs seeded with M0 macrophages secreted significantly higher amounts of glycerol than all other groups. Constructs from the third patient (**Figure 20C**) displayed similar trends to patient 2 without the change at day 28. Consistent with enhanced triglyceride accumulation and increased leptin secretion, the magnitude of glycerol secretion from Patient 3 was higher than the other patients. Glycerol secretion tended to decrease over time in all groups.

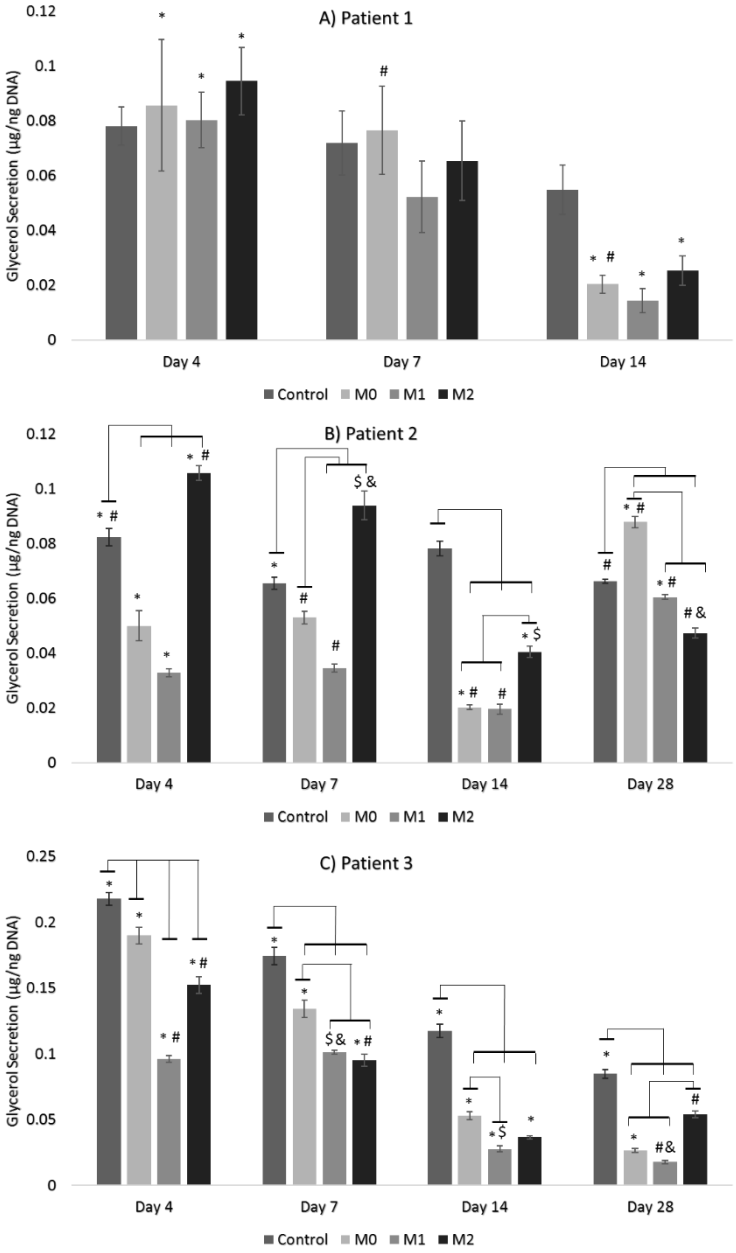

Figure 20. Glycerol secretion of the constructs was determined at different timepoints and among different culture conditions and normalized by DNA content to quantify the extent of lipolysis. A 2 way ANOVA was performed where the factors were the time cultured and the type of macrophage seeded onto the scaffolds. Constructs using the sample of Patient 1 (**A**) did not display a significant effect of the factors interacting, but did vary over time ($p<0.0001$). Constructs using samples Patients 2 and 3 (**B** and **C)** did display a significant effect of the two factors interacting ($p<0.0001$). A Tukey post hoc test was performed for significant factors and interactions. Significance between macrophage seeding groups within certain timepoints are denoted by lines connecting them. Significance between timepoints within the same macrophage seeding group is denoted by a shared symbol. Significance was defined as $p<0.05$. Samples were run in duplicate with at least n=5. Error bars represent standard error of the mean.

4.2.5. Confocal Imaging

Samples were fixed for confocal imaging at all four timepoints for the last two patients (**Figure 21** and **Figure 22**). Immunohistochemistry was used to stain for the macrophage marker CD68, and the cell nuclei were stained with DAPI. Coherent anti-Stokes Raman spectroscopy was simultaneously used to image lipids. The CD68 staining was used to determine if the seeded macrophages survived throughout the experimentation. The images confirm the trends seen in DNA content quantification as increased levels of DAPI signal was seen over time and in the constructs seeded with macrophages. CD68 signal was seen in the later timepoints, but it is unclear if it was background from the increased proliferation as it was also seen in the control group.

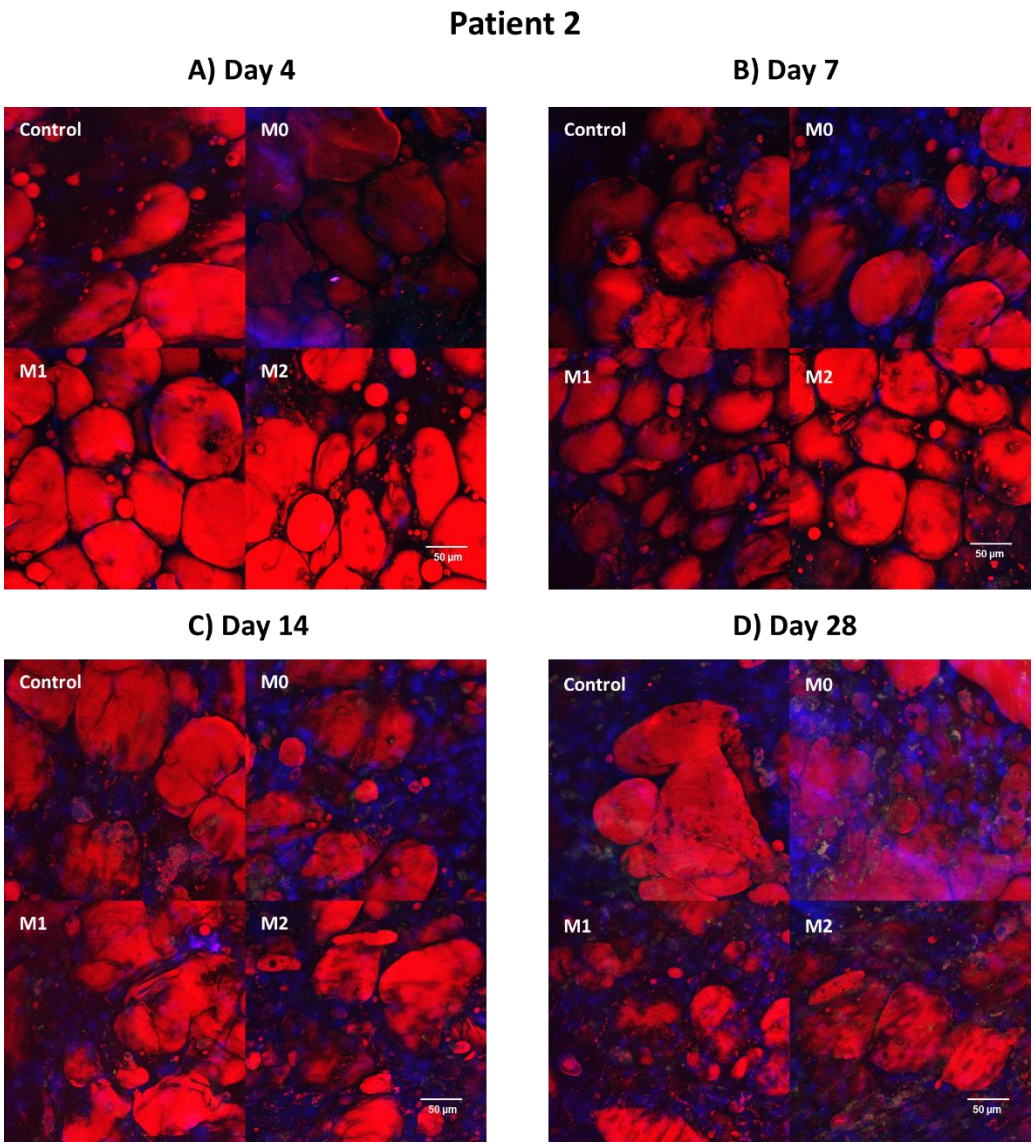

Figure 21. Fluorescent images of the adipose constructs using samples from Patient 2 were taken with a confocal microscope at four different timepoints (4 days, 7 days, 14 days, and 28 days). Cells were stained with DAPI (blue) to denote cell nuclei and CD68 (green), a macrophage marker. Coherent anti-Stokes Raman spectroscopy was simultaneously used to image the lipids within the cells (red).

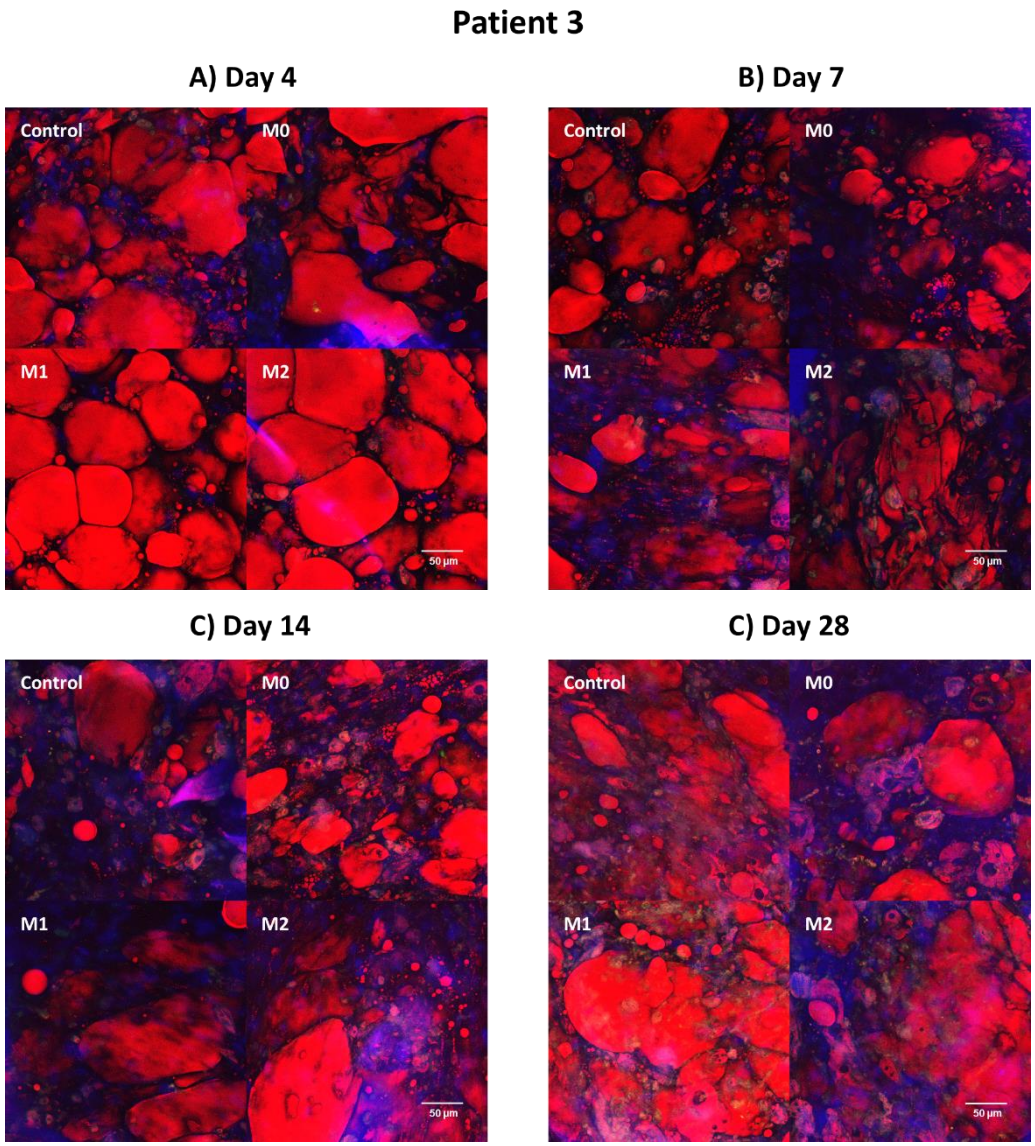

Figure 22. Fluorescent images of the adipose constructs using samples from Patient 3 were taken with a confocal microscope at four different timepoints (4 days, 7 days, 14 days, and 28 days). Cells were stained with DAPI (blue) to denote cell nuclei and CD68 (green), a macrophage marker. Coherent anti-Stokes Raman spectroscopy was simultaneously used to image the lipids within the cells (red).

4.3. Aim 3: Inducing an acute inflammatory response in adipose constructs

A preliminary experiment attempting to induce an acute inflammatory response in the adipose constructs as opposed to a chronic response was conducted. The constructs (using a fourth adipose sample) were stimulated by different concentrations of lipopolysaccharide and assessed based on DNA content and glycerol secretion.

4.3.1 DNA Content

Immediately after LPS stimulation (day 1), constructs exposed to 1 µg/ml LPS showed a significant increase in DNA content when compared to the control (**Figure 23A**). By day 4, the constructs exposed to the same concentration decreased back to a magnitude similar to the other groups. Otherwise, LPS stimulation had little effect on DNA content of the constructs.

4.3.2. Glycerol Secretion

LPS stimulation had a larger effect on glycerol secretion (**Figure 23B**). At day 4, constructs exposed to 1 µg/ml LPS exhibited increased glycerol secretion when compared to the other groups. However, by days 7 and 14, the control group displayed higher levels of secretion than the two groups stimulated with LPS. Among all groups, glycerol secretion tended to increase with time.

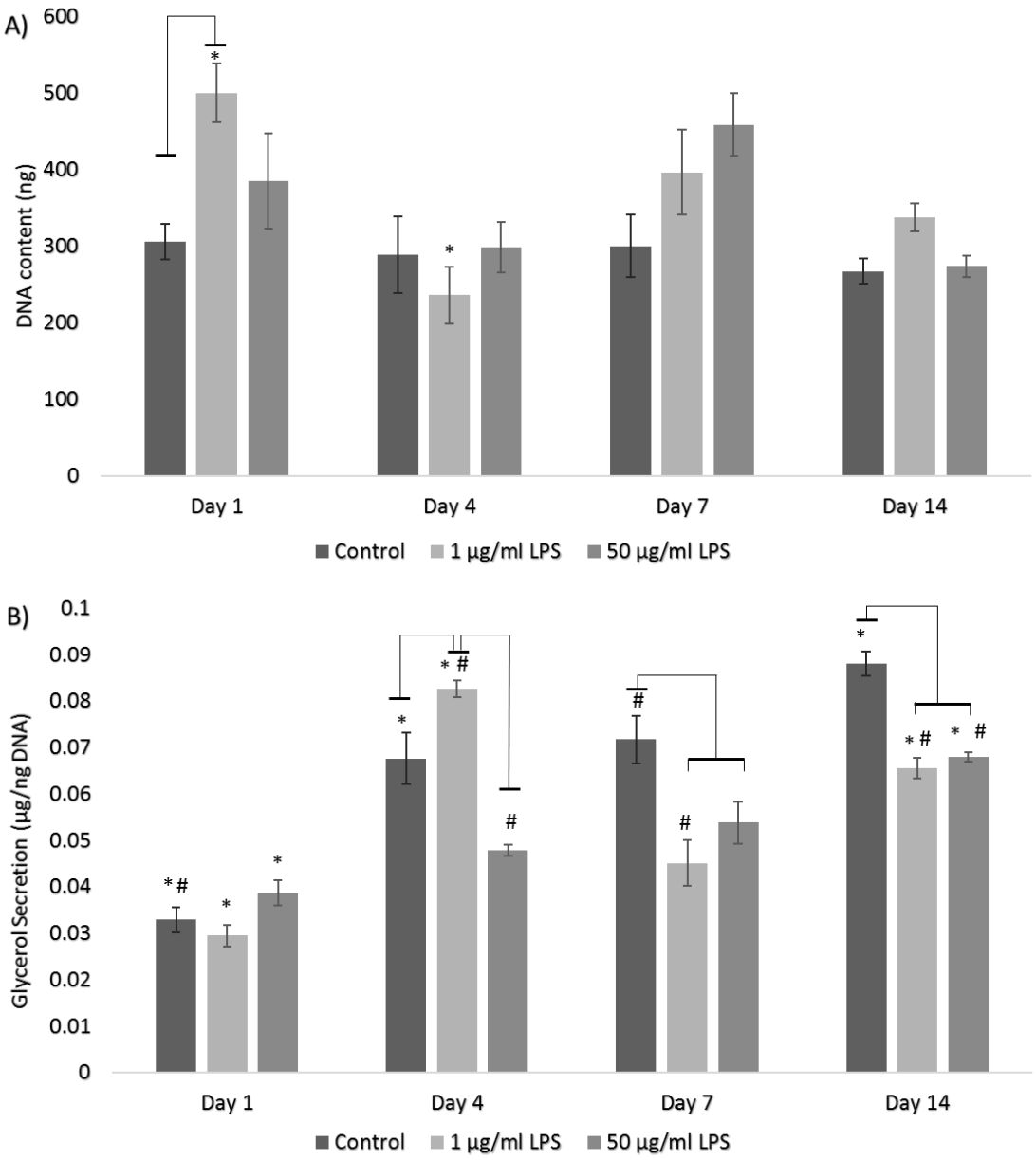

Figure 23. DNA content (A) and glycerol secretion (B) of the constructs were determined at different timepoints and among different culture conditions. Glycerol secretion was normalized by DNA content to quantify the extent of lipolysis. A 2 way ANOVA was performed where the factors were the time cultured and the concentration of LPS used. Both DNA content and glycerol secretion displayed a significant effect of the two factors interacting ($p=0.0284$ for DNA and $p<0.0001$ for glycerol). A Tukey post hoc test was performed for significant factors and interactions. Significance between LPS concentration within certain timepoints are denoted by lines connecting them. Significance between timepoints within the same LPS concentration group is denoted by a shared symbol. Significance was defined as $p<0.05$. Samples were run in duplicate with at least $n=5$. Error bars represent standard error of the mean.

5. Discussion

The study set out to induce an inflammatory state in a three-dimensional *in vitro* adipose model to mimic the inflammatory phenotype seen in obesity. The majority of the work focused on simulating immune cell infiltration seen in obesity to achieve an inflammatory state in three-dimensional adipose constructs. Preliminary work was also done in attempting to recapitulate an acute inflammatory response in the same adipose constructs.

The THP-1 cell line was chosen as the potential source instead of primary macrophages since primary macrophages cannot be expanded *ex vivo* and have a very limited lifespan in culture (Lund et al., 2016). THP-1 cells can be continually expanded during experimentation, and the THP-1 monocytes can be differentiated into macrophages and further polarized towards M1 and M2 states (Chanput et al., 2013). The first portion of the work confirmed this ability. The images seen in **Figure 14** and **Figure 15** illustrate that the THP-1 monocytes were successfully differentiated into macrophages. Furthermore, the ability to further polarize the macrophages was confirmed using RT-qPCR (**Figure 16**). Interestingly, the M1 polarized macrophages displayed an increase in lipid content in the images taken. LPS (one of the two components added to polarize the THP1 macrophage toward the M1 state) has been shown to induce the formation of foam cells (Feng et al., 2014). Foam cells are macrophages that have accumulated lipids and are influential at all stages of atherosclerosis (Valledor et al., 2001). This trait can be particularly useful for identifying macrophages non-invasively with CARS.

Before experimentation, it was hypothesized that the simulation of immune cell infiltration would induce an inflammatory state mimicking obesity. As obesity progresses, basal lipolysis rates and leptin production increase (Duncan et al., 2007, Bai and Sun, 2015). Therefore, it was expected that the adipose constructs seeded with macrophages would mimic

these phenomena. Additionally, it was expected that the M1-polarized macrophages would induce the greatest effect since they are identified by increased proinflammatory cytokines (Chanput et al., 2013). However, the results were mixed and varied depending on which patient the adipose samples were obtained from.

Differences among patients in response to the immune cells can first be seen when quantifying the DNA content (**Figure 17)**. Samples from Patient 1 showed no significant differences in proliferation in response to the seeding of macrophages (**Figure 17A**). However, after two weeks of culture, samples from the other two patients had enhanced proliferation in response to the macrophages, most noticeably from the seeding of M0 "resting" macrophages (**Figure 17B** and **Figure 17C**)**.** Confocal imaging (**Figure 21** and **Figure 22**) showed similar trends of increased proliferation. In a 2D co-culture study, addition of THP-1 macrophages resulted in increased rates of adipocyte apoptosis (Keuper et al., 2011), but the added dimensionality and cell types of this model could account for the observed difference. Obesity is marked by the enlargement of adipose tissue, and there are two possible ways for adipose tissue to grow: hyperplasia (increase in cell number) and hypertrophy (increase in cell size) (Jo et al., 2009). The increased proliferation demonstrated by the constructs seeded with macrophages mimics the hyperplasic trend seen in obesity.

Triglyceride content (which was normalized by DNA content) (**Figure 18**) was largely dependent on its corresponding DNA content. Constructs with increased levels of DNA content displayed decreases in normalized triglyceride content. Obesity promotes the accumulation of triglycerides, and hypertrophy is needed to account for the increased accumulation by increasing adipocytes' storage capacity (Bolsoni-Lopes et al., 2015; Jo et al., 2009). These results suggest that the proliferating cells associated with the seeding of macrophages are not accumulating

triglycerides which demonstrates that exposure to macrophages alone does not promote triglyceride accumulation.

Production of leptin increases in the adipose tissue of obese patients (Bai and Sun, 2015). It was hypothesized that the addition of macrophages to the adipose constructs would mirror this trend. Again, variability among samples from different patients was evident. When assessing leptin secretion (**Figure 19)**, the control groups from all patient samples either remained relatively constant or decreased over time, but the addition of macrophages showed increases in secretion. Although hypothesized that M1-polarized macrophages would elicit the largest effect, that was not always the case. Samples from Patient 2 (**Figure 19B**) reacted most strongly to the addition of the M0 "resting" macrophages, for instance. Patient 3 samples (**Figure 19C**) exhibited the hypothesized response as M1-polarized macrophages tended to induce the largest amount of leptin production with M0 macrophages also inducing a significant response.

As M0 macrophages have not been polarized prior to seeding, they may have been influenced by their environment in the adipose construct causing the strong response in Patient 2 and also the still significant response in Patient 3. This would not be unprecedented as it has been demonstrated that the macrophage's environment could promote a transition from the M2 to M1 state in obesity (Lumeng et al., 2007). As the M0 resting state is already prone to polarization based on stimuli, it is likely that the macrophages may have been polarized toward the proinflammatory M1 state due to their environment. Interestingly, Patient 2 was the only non-obese patient, having a normal BMI of 24.1. One would expect that the environment that would push the M0 macrophages towards M1 to be that of an obese patient.

Basal lipolysis rates increase in obese patients (Duncan et al., 2007), so it was hypothesized that glycerol secretion would increase with the addition of macrophages. When

assessing glycerol secretion (**Figure 20**), the trends among patients were actually similar before the final timepoints. In general, constructs seeded with M0 and M1 macrophages (which tended to have increased leptin production), secreted less glycerol than their control group counterparts, contrary to the hypothesis. However, Patient 2 (**Figure 20B**) displayed a change at day 28 where constructs seeded with M0 macrophages secreted the largest amount of glycerol and those seeded with M1 macrophages were no longer secreting significantly lower amounts than the control. It is possible that the other patient samples would have also displayed this delayed effect if they had been allowed to culture for a longer period. As obesity is a chronic condition, this delayed response may be favorable to the more immediate response demonstrated in leptin production (**Figure 19**).

The likely explanation for seeing the delayed response in lipolytic changes sooner in the second patient's constructs is its relative leptin production. Increased leptin production *in vivo* eases transport of macrophages to adipose tissue and promotes attachment of macrophages to endothelial cells (Wellen and Hotamisligil, 2003). The constructs seeded with M0 macrophages displayed significantly higher leptin production than the other groups in the earlier timepoints. The more immediate leptin response may have created a more welcoming environment for the macrophages seeded in subsequent weeks which, in turn, led to the delayed spike in glycerol secretion.

The preliminary work attempting to induce an acute inflammatory response assessed the glycerol secretion and the DNA content of the constructs after being exposed to lipopolysaccharide. As exposure to LPS has been shown to upregulate the secretion of proinflammatory cytokines (Ibisch et al., 2007), it was hypothesized that that upregulation would influence lipolysis rates. Lipopolysaccharide stimulation successfully induced an increased

lipolytic response when exposed to the "low" concentration at day 4 (**Figure 23)**. As the aim was to achieve an acute response, the increase at the earlier timepoint was the expected outcome.

Taken together, the results indicate that patient specific differences played a major role in how the constructs responded to a chronic inflamed state. The outputs of the different patient samples showed both different trends as well as different magnitudes. For example, Patient 3 exhibited much larger levels of triglyceride content, leptin production, and glycerol secretion (**Figure 18, Figure 19,** and **Figure 20**). The higher triglyceride content suggests Patient 3's constructs consisted of more lipid laden cells which was likely the reason for the corresponding leptin and glycerol secretion magnitudes to also be relatively high. Variability among different patient samples is not necessarily unexpected; a study using the same model demonstrated variability in both lipolytic responses and glucose uptake among different samples (Abbott et al., Submitted). Although this variability among patients makes reproducing experiments using this model more difficult, it highlights one of its major advantages. The human population is complex and widely different depending on factors such as genetics, ethnicity, lifestyle, sex, height, and weight. For example, the composition of adipose tissue (both in terms of cell type percentages and structure) vary person to person (Curat et al., 2006; van Harmelen et al.; 2003, Divoux et al., 2010). Having a patient specific model is widely beneficial when trying to understand how a patient will react to different stimuli, including chronic inflammation.

6. Conclusions and Future Directions

The overall goal of this thesis was to induce an inflammatory state in an *in vitro* three-dimensional adipose disease model mimicking obesity. The model will be beneficial in the efforts to better understand obesity and to test strategies in preventing and treating the influential disease. The work simulating infiltration of immune cells into the construct was successful in demonstrating different aspects of the obese phenotype while also highlighting the variability of different patients.

6.1. Future Directions

To contribute more to the immune cell infiltration work, different aspects of the experimental design can be built upon. For instance, increasing culture time of the constructs (as long as 2-3 months) would provide a more complete assessment of the model. As obesity is a chronic condition, 28 days may not have been sufficient for the constructs demonstrate their response in a measurable manner. For instance, Patient 2 demonstrated a delayed upregulation of glycerol secretion at day 28 (**Figure 20**), but exhibited similar trends to the other two patients before that timepoint. The other patient samples may have also displayed that same delayed response (or a different response) if given enough time to culture.

Additionally, quantification of MCP-1 secretion of the adipose constructs using an ELISA would provide an output specific to the mechanism behind the recruitment of macrophages to the adipose tissue. As MCP-1 activates resident macrophages and further recruits immune cells to adipose tissue *in vivo* (Bai and Sun, 2015), quantifying the release of the cytokine would offer a better understanding of how the adipose constructs and the exogenous macrophages are interacting.

Another direction to pursue would be culturing the constructs in a white adipose tissue differentiation media in tandem with the addition of macrophages. Without the addition of macrophages, using a differentiation media supplemented with IBMX, indomethacin, dexamethasone, and insulin, the construct demonstrated increased lipid accumulation and glycerol secretion with reduced proliferation as preadipocytes are differentiated into mature adipocytes (Abbott et al., 2016). The hypothesis is that combining the proliferative effects of the addition of macrophages with the differentiation media will result in a synergistic effect and a greater inflammatory response.

One study utilized Transwell inserts to assess the effects of THP-1 macrophage secretions on melanoma cells while avoiding direct cell contact (Smith et al., 2014). Assessing the difference between direct exposure to macrophages and indirect exposure may expose different trends in the adipose constructs. The Transwell inserts would allow the adipose construct and the supplemented macrophages to be physically separated to be able to assess if secreted cytokines alone would induce an inflammatory response or if the direct seeding of the macrophages is needed.

To further the LPS acute inflammation stimulation experiment, additional outputs such as leptin secretion, adiponectin secretion, and triglyceride content can be assessed. Additionally, further varying LPS stimulation concentration while varying time stimulated may also impact the outcomes. Assessing other inflammatory stimulants such interleukin-1 (IL-1) (Dinarello 2000) is another viable option.

In a broader scope, the inflammatory model simulating immune cell infiltration would benefit from assessing a large spectrum of different patients. It was evident that different patients responded differently. As the information received about each patient is very limited, any

correlations found between measurable baseline characteristics (like relative amounts of lipid laden cells determined by triglyceride content) and response to inflammation could prove to be vital. Chronic inflammation from obesity does not affect all equally. Obesity can cause insulin resistance and type 2 diabetes, but not all obese patients suffer from these conditions (Kahn and Flier, 2000). For example, the samples from patient 1 were not as responsive (regardless of condition) to the simulated inflammation when compared to the other two patients. With a large enough accumulation of patient specific data, the hope is to find patterns that can help better understand why different patients handle inflammation differently.

To this end, each patient's lipoaspirate sample can be analyzed to determine both the different cell types in each as well as their relative abundance using fluorescence activated cell sorting (FACS). As the percentage of the different cell types varies from person to person, knowing the composition of each patient's adipose tissue would provide crucial baseline data that could help parse the variation seen between different patient samples. The data can also be used as a better way to normalize responses rather than just using overall DNA content.

References

Abbott, Rosalyn D., Francis E. Borowsky, Kyle P. Quinn, David L. Bernstein, Irene Georgakoudi, and David L. Kaplan. 2015. “Non-Invasive Assessments of Adipose Tissue Metabolism In Vitro.” *Annals of Biomedical Engineering* 44 (3): 725–32. doi:10.1007/s10439-015-1438-9.

Abbott, Rosalyn D., Francis E. Borowsky, Adam Zieba, Carlo A. Alonzo, Irene Georgakoudi, and David L. Kaplan. “An *in vitro* human white adipose tissue engineered model that accounts for human variability” Submitted.

Abbott, Rosalyn D., Rebecca Y. Wang, Michaela R. Reagan, Ying Chen, Francis E. Borowsky, Adam Zieba, Kacey G. Marra, J. Peter Rubin, Irene M. Ghobrial, and David L. Kaplan. 2016. “The Use of Silk as a Scaffold for Mature, Sustainable Unilocular Adipose 3D Tissue Engineered Systems.” *Advanced Healthcare Materials*, May, n/a-n/a. doi:10.1002/adhm.201600211.

Ahima, Rexford S., and Mitchell A. Lazar. 2013. “The Health Risk of Obesity—Better Metrics Imperative.” *Science* 341 (6148): 856–58. doi:10.1126/science.1241244.

Aubin, Kim, Meryem Safoine, Maryse Proulx, Marie-Alice Audet-Casgrain, Jean-François Côté, Félix-André Têtu, Alphonse Roy, and Julie Fradette. 2015. “Characterization of In Vitro Engineered Human Adipose Tissues: Relevant Adipokine Secretion and Impact of TNF-α.” *PLOS ONE* 10 (9): e0137612. doi:10.1371/journal.pone.0137612.

Bai, Y., and Q. Sun. 2015. “Macrophage Recruitment in Obese Adipose Tissue.” *Obesity Reviews* 16 (2): 127–36. doi:10.1111/obr.12242.

Bellas, Evangelia, Kacey G. Marra, and David L. Kaplan. 2013. “Sustainable Three-Dimensional Tissue Model of Human Adipose Tissue.” *Tissue Engineering. Part C, Methods* 19 (10): 745–54. doi:10.1089/ten.tec.2012.0620.

Bolsoni-Lopes, Andressa, Maria Isabel C. Alonso-Vale, Andressa Bolsoni-Lopes, and Maria Isabel C. Alonso-Vale. 2015a. “Lipolysis and Lipases in White Adipose Tissue – An Update.” *Archives of Endocrinology and Metabolism* 59 (4): 335–42. doi:10.1590/2359-3997000000067.

Bouillon, Roger, Geert Carmeliet, Liesbet Lieben, Mitsuhiro Watanabe, Alessia Perino, Johan Auwerx, Kristina Schoonjans, and Annemieke Verstuyf. 2014. “Vitamin D and Energy Homeostasis—of Mice and Men.” *Nature Reviews Endocrinology* 10 (2): 79–87. doi:10.1038/nrendo.2013.226.

Bradley, Richard L., Ffolliott M. Fisher, and Eleftheria Maratos-Flier. 2008. “Dietary Fatty Acids Differentially Regulate Production of TNF-α and IL-10 by Murine 3T3-L1 Adipocytes.” *Obesity (Silver Spring, Md.)* 16 (5): 938–44. doi:10.1038/oby.2008.39.

Chanput, Wasaporn, Jurriaan J. Mes, Huub F. J. Savelkoul, and Harry J. Wichers. 2013. "Characterization of Polarized THP-1 Macrophages and Polarizing Ability of LPS and Food Compounds." *Food & Function* 4 (2): 266–76. doi:10.1039/C2FO30156C.

Chanput, Wasaporn, Jurriaan Mes, Robert A. M. Vreeburg, Huub F. J. Savelkoul, and Harry J. Wichers. 2010. "Transcription Profiles of LPS-Stimulated THP-1 Monocytes and Macrophages: A Tool to Study Inflammation Modulating Effects of Food-Derived Compounds." *Food & Function* 1 (3): 254–61. doi:10.1039/C0FO00113A.

Curat, C. A., V. Wegner, C. Sengenès, A. Miranville, C. Tonus, R. Busse, and A. Bouloumié. 2006a. "Macrophages in Human Visceral Adipose Tissue: Increased Accumulation in Obesity and a Source of Resistin and Visfatin." *Diabetologia* 49 (4): 744–47. doi:10.1007/s00125-006-0173-z.

Castells-Sala C, Alemany-Ribes M, Fernandez-Muiños T, Recha-Sancho L, Lopez-Chicon P et al. "Current Applications of Tissue Engineering in Biomedicine." 2013. *Journal of Biochips & Tissue Chips*, August, 1–14. doi:10.4172/2153-0777.S2-004.

Daemen, Sabine, Marc A. M. J. van Zandvoort, Sapun H. Parekh, and Matthijs K. C. Hesselink. 2016. "Microscopy Tools for the Investigation of Intracellular Lipid Storage and Dynamics." *Molecular Metabolism* 5 (3): 153–63. doi:10.1016/j.molmet.2015.12.005.

Dillingh, Marlous R., Eveline P. van Poelgeest, Karen E. Malone, Elles M. Kemper, Erik S. G. Stroes, Matthijs Moerland, and Jacobus Burggraaf. 2014. "Characterization of Inflammation and Immune Cell Modulation Induced by Low-Dose LPS Administration to Healthy Volunteers." *Journal of Inflammation* 11: 28. doi:10.1186/s12950-014-0028-1.

Dinarello, Charles A. 2000. "Proinflammatory Cytokines." *Chest* 118 (2): 503–8. doi:10.1378/chest.118.2.503.

Divoux, Adeline, Joan Tordjman, Danièle Lacasa, Nicolas Veyrie, Danielle Hugol, Abdelhalim Aissat, Arnaud Basdevant, et al. 2010a. "Fibrosis in Human Adipose Tissue: Composition, Distribution, and Link With Lipid Metabolism and Fat Mass Loss." *Diabetes* 59 (11): 2817–25. doi:10.2337/db10-0585.

Duncan, Robin E., Maryam Ahmadian, Kathy Jaworski, Eszter Sarkadi-Nagy, and Hei Sook Sul. 2007. "Regulation of Lipolysis in Adipocytes." *Annual Review of Nutrition* 27: 79–101. doi:10.1146/annurev.nutr.27.061406.093734.

Edmondson, Rasheena, Jessica Jenkins Broglie, Audrey F. Adcock, and Liju Yang. 2014. "Three-Dimensional Cell Culture Systems and Their Applications in Drug Discovery and Cell-Based Biosensors." *Assay and Drug Development Technologies* 12 (4): 207–18. doi:10.1089/adt.2014.573.

Fantuzzi, Giamila. 2005. “Adipose Tissue, Adipokines, and Inflammation.” *Journal of Allergy and Clinical Immunology* 115 (5): 911–19. doi:10.1016/j.jaci.2005.02.023.

Feng, Xuyang, Yuan Yuan, Chao Wang, Jun Feng, Zuyi Yuan, Xiumin Zhang, Wen Sui, Peizhen Hu, Pengfei Zheng, and Jing Ye. 2014. “Autophagy Involved in Lipopolysaccharide-Induced Foam Cell Formation Is Mediated by Adipose Differentiation-Related Protein.” *Lipids in Health and Disease* 13 (January): 10. doi:10.1186/1476-511X-13-10.

Fraternale, A, S Brundu, and M Magnani. 2014. “Polarization and Repolarization of Macrophages.” *Journal of Clinical & Cellular Immunology* 6 (2): 1–10. doi:10.4172/2155-9899.1000319.

Genin, Marie, Francois Clement, Antoine Fattaccioli, Martine Raes, and Carine Michiels. 2015. “M1 and M2 Macrophages Derived from THP-1 Cells Differentially Modulate the Response of Cancer Cells to Etoposide.” *BMC Cancer* 15: 577. doi:10.1186/s12885-015-1546-9.

Gerlach, Jörg C., Yen-Chih Lin, Candace A. Brayfield, Danielle M. Minteer, Han Li, J. Peter Rubin, and Kacey G. Marra. 2012. “Adipogenesis of Human Adipose-Derived Stem Cells Within Three-Dimensional Hollow Fiber-Based Bioreactors.” *Tissue Engineering. Part C, Methods* 18 (1): 54–61. doi:10.1089/ten.tec.2011.0216.

Griffith, Linda G., and Gail Naughton. 2002. “Tissue Engineering--Current Challenges and Expanding Opportunities.” *Science* 295 (5557): 1009–14. doi:10.1126/science.1069210.

Hammond, Ross A, and Ruth Levine. 2010. “The Economic Impact of Obesity in the United States.” *Diabetes, Metabolic Syndrome and Obesity : Targets and Therapy* 3 (August): 285–95. doi:10.2147/DMSOTT.S7384.

Harmelen, V. van, T. Skurk, K. Röhrig, Y.-M. Lee, M. Halbleib, I. Aprath-Husmann, and H. Hauner. 2003. “Effect of BMI and Age on Adipose Tissue Cellularity and Differentiation Capacity in Women.” *International Journal of Obesity and Related Metabolic Disorders: Journal of the International Association for the Study of Obesity* 27 (8): 889–95. doi:10.1038/sj.ijo.0802314.

Ibisch, C., P. Bourdeau, C. Cadiot, J. Viac, and H. Gatto. 2007. “Upregulation of TNF-α Production by IFN-γ and LPS in Cultured Canine Keratinocytes: Application to Monosaccharides Effects.” *Veterinary Research Communications* 31 (7): 835–46. doi:10.1007/s11259-007-0004-9.

Jo, Junghyo, Oksana Gavrilova, Stephanie Pack, William Jou, Shawn Mullen, Anne E. Sumner, Samuel W. Cushman, and Vipul Periwal. 2009. “Hypertrophy And/or Hyperplasia: Dynamics of Adipose Tissue Growth.” *PLoS Computational Biology* 5 (3). doi:10.1371/journal.pcbi.1000324.

Kahn, Barbara B., and Jeffrey S. Flier. 2000. “Obesity and Insulin Resistance.” *Journal of Clinical Investigation* 106 (4): 473–81.

Kang, Jennifer H., Jeffrey M. Gimble, and David L. Kaplan. 2009. “In Vitro 3D Model for Human Vascularized Adipose Tissue.” *Tissue Engineering. Part A* 15 (8): 2227–36. doi:10.1089/ten.tea.2008.0469.

Keuper, Michaela, Matthias Blüher, Michael R. Schön, Peter Möller, Anna Dzyakanchuk, Kurt Amrein, Klaus-Michael Debatin, Martin Wabitsch, and Pamela Fischer-Posovszky. 2011. “An Inflammatory Micro-Environment Promotes Human Adipocyte Apoptosis.” *Molecular and Cellular Endocrinology* 339 (1–2): 105–13. doi:10.1016/j.mce.2011.04.004.

Kopelman, P. 2007. “Health Risks Associated with Overweight and Obesity.” *Obesity Reviews* 8 (March): 13–17. doi:10.1111/j.1467-789X.2007.00311.x.

Lehnert, Thomas, Diana Sonntag, Alexander Konnopka, Steffi Riedel-Heller, and Hans-Helmut König. 2013. “Economic Costs of Overweight and Obesity.” *Best Practice & Research Clinical Endocrinology & Metabolism*, Complications of Obesity, 27 (2): 105–15. doi:10.1016/j.beem.2013.01.002.

Lo, Kinyui Alice, Adam Labadorf, Norman J. Kennedy, Myoung Sook Han, Yoon Sing Yap, Bryan Matthews, Xiaofeng Xin, et al. 2013. “Analysis of in Vitro Insulin Resistance Models and Their Physiological Relevance to in Vivo Diet-Induced Adipose Insulin Resistance.” *Cell Reports* 5 (1). doi:10.1016/j.celrep.2013.08.039.

Lumeng, Carey N., Jennifer L. Bodzin, and Alan R. Saltiel. 2007. “Obesity Induces a Phenotypic Switch in Adipose Tissue Macrophage Polarization.” *The Journal of Clinical Investigation* 117 (1): 175–84. doi:10.1172/JCI29881.

Lund, Maria E., Joyce To, Bronwyn A. O’Brien, and Sheila Donnelly. 2016. “The Choice of Phorbol 12-Myristate 13-Acetate Differentiation Protocol Influences the Response of THP-1 Macrophages to a pro-Inflammatory Stimulus.” *Journal of Immunological Methods* 430 (March): 64–70. doi:10.1016/j.jim.2016.01.012.

Mantovani, Alberto, Antonio Sica, Silvano Sozzani, Paola Allavena, Annunciata Vecchi, and Massimo Locati. 2004. “The Chemokine System in Diverse Forms of Macrophage Activation and Polarization.” *Trends in Immunology* 25 (12): 677–86. doi:10.1016/j.it.2004.09.015.

Martinez, Fernando O., and Siamon Gordon. 2014. “The M1 and M2 Paradigm of Macrophage Activation: Time for Reassessment.” *F1000Prime Reports* 6 (March). doi:10.12703/P6-13.

Martinez, Fernando O., Siamon Gordon, Massimo Locati, and Alberto Mantovani. 2006. “Transcriptional Profiling of the Human Monocyte-to-Macrophage Differentiation and

Polarization: New Molecules and Patterns of Gene Expression." *The Journal of Immunology* 177 (10): 7303–11. doi:10.4049/jimmunol.177.10.7303.

Martinez, Fernando O., Laura Helming, and Siamon Gordon. 2009. "Alternative Activation of Macrophages: An Immunologic Functional Perspective." *Annual Review of Immunology* 27 (1): 451–83. doi:10.1146/annurev.immunol.021908.132532.

Medzhitov, Ruslan. 2008. "Origin and Physiological Roles of Inflammation." *Nature* 454 (7203): 428–35. doi:10.1038/nature07201.

Metukuri, Mallikarjuna Reddy, Chandra Mohan T. Reddy, P. R. K. Reddy, and Pallu Reddanna. 2010. "Bacterial LPS Mediated Acute Inflammation-Induced Spermatogenic Failure in Rats: Role of Stress Response Proteins and Mitochondrial Dysfunction." *Inflammation* 33 (4): 235–43. doi:10.1007/s10753-009-9177-4.

Murakami, Masaaki, and Toshio Hirano. 2012. "The Molecular Mechanisms of Chronic Inflammation Development." *Frontiers in Immunology* 3 (November). doi:10.3389/fimmu.2012.00323.

Nerem, Robert M., and Athanassios Sambanis. 1995. "Tissue Engineering: From Biology to Biological Substitutes." *Tissue Engineering* 1 (1): 3–13. doi:10.1089/ten.1995.1.3.

Ogden CL, Carroll MD, Kit BK, and Flegal KM. 2014. "PRevalence of Childhood and Adult Obesity in the United States, 2011-2012." *JAMA* 311 (8): 806–14. doi:10.1001/jama.2014.732.

Park, E. K., H. S. Jung, H. I. Yang, M. C. Yoo, C. Kim, and K. S. Kim. 2007. "Optimized THP-1 Differentiation Is Required for the Detection of Responses to Weak Stimuli." *Inflammation Research* 56 (1): 45–50. doi:10.1007/s00011-007-6115-5.

Pezacki, John Paul, Jessie A. Blake, Dana C. Danielson, David C. Kennedy, Rodney K. Lyn, and Ragunath Singaravelu. 2011. "Chemical Contrast for Imaging Living Systems: Molecular Vibrations Drive CARS Microscopy." *Nature Chemical Biology* 7 (3): 137–45. doi:10.1038/nchembio.525.

Rockwood, Danielle N., Rucsanda C. Preda, Tuna Yücel, Xiaoqin Wang, Michael L. Lovett, and David L. Kaplan. 2011. "Materials Fabrication from Bombyx Mori Silk Fibroin." *Nature Protocols* 6 (10): 1612–31. doi:10.1038/nprot.2011.379.

"Sandwich ELISA Platform Overview" *LifeSpan Biosciences, Inc.* https://www.lsbio.com/elisakits/human-cortisol-elisa-kit-sandwich-elisa-ls-f26720/26720

Serhan, Charles N., Peter A. Ward, and Derek W. Gilroy. 2010. *Fundamentals of Inflammation*. Cambridge University Press.

Serlachius, Martina, and Leif C Andersson. 2004. "Upregulated Expression of Stanniocalcin-1

during Adipogenesis." *Experimental Cell Research* 296 (2): 256–64. doi:10.1016/j.yexcr.2004.02.016.

Smith, Michael P., Berta Sanchez-Laorden, Kate O'Brien, Holly Brunton, Jennifer Ferguson, Helen Young, Nathalie Dhomen, et al. 2014. "The Immune-Microenvironment Confers Resistance to MAP Kinase Pathway Inhibitors through Macrophage-Derived TNFα." *Cancer Discovery* 4 (10): 1214–29. doi:10.1158/2159-8290.CD-13-1007.

Sugihara, Hajime, Nobuhisa Yonemitsu, Shinichi Miyabara, and Kankatsu Yun. 1986. "Primary Cultures of Unilocular Fat Cells: Characteristics of Growth in Vitro and Changes in Differentiation Properties." *Differentiation* 31 (1): 42–49. doi:10.1111/j.1432-0436.1986.tb00381.x.

Swinburn, Boyd A, Gary Sacks, Kevin D Hall, Klim McPherson, Diane T Finegood, Marjory L Moodie, and Steven L Gortmaker. 2011. "The Global Obesity Pandemic: Shaped by Global Drivers and Local Environments." *The Lancet* 378 (9793): 804–14. doi:10.1016/S0140-6736(11)60813-1.

Toda, Shuji, Kazuyoshi Uchihashi, Shigehisa Aoki, Emiko Sonoda, Fumio Yamasaki, Meihua Piao, Akifumi Ootani, Nobuhisa Yonemitsu, and Hajime Sugihara. 2009. "Adipose Tissue-Organotypic Culture System as a Promising Model for Studying Adipose Tissue Biology and Regeneration." *Organogenesis* 5 (2): 50–56.

Trayhurn, Paul, and John H. Beattie. 2001. "Physiological Role of Adipose Tissue: White Adipose Tissue as an Endocrine and Secretory Organ." *Proceedings of the Nutrition Society* 60 (3): 329–39. doi:10.1079/PNS200194.

Tulk, Sarah E., Kuo-Chieh Liao, Daniel A. Muruve, Yan Li, Paul L. Beck, and Justin A. MacDonald. 2015. "Vitamin D3 Metabolites Enhance the NLRP3-Dependent Secretion of IL-1β From Human THP-1 Monocytic Cells." *Journal of Cellular Biochemistry* 116 (5): 711–20. doi:10.1002/jcb.24985.

Turner, Paul A., Yi Tang, Stephen J. Weiss, and Amol V. Janorkar. 2015. "Three-Dimensional Spheroid Cell Model of In Vitro Adipocyte Inflammation." *Tissue Engineering Part A* 21 (11–12): 1837–47. doi:10.1089/ten.tea.2014.0531.

Valledor, Annabel F, Jorge Lloberas, and Antonio Celada. 2001. "Macrophage Foam Cells." In *eLS*. John Wiley & Sons, Ltd. http://onlinelibrary.wiley.com/doi/10.1002/9780470015902.a0020730.pub2/abstract.

Vepari, Charu, and David L. Kaplan. 2007. "Silk as a Biomaterial." *Progress in Polymer Science* 32 (8–9): 991–1007. doi:10.1016/j.progpolymsci.2007.05.013.

Vistisen, Dorte, Daniel R. Witte, Adam G. Tabák, Christian Herder, Eric J. Brunner, Mika Kivimäki, and Kristine Færch. 2014. "Patterns of Obesity Development before the Diagnosis of Type 2 Diabetes: The Whitehall II Cohort Study." *PLOS Medicine* 11 (2):

e1001602. doi:10.1371/journal.pmed.1001602.

Vogel, Daphne Y. S., Judith E. Glim, Andrea W. D. Stavenuiter, Marjolein Breur, Priscilla Heijnen, Sandra Amor, Christine D. Dijkstra, and Robert H. J. Beelen. 2014. "Human Macrophage Polarization in Vitro: Maturation and Activation Methods Compared." *Immunobiology* 219 (9): 695–703. doi:10.1016/j.imbio.2014.05.002.

Wang, Rebecca Y., Rosalyn D. Abbott, Adam Zieba, Francis E. Borowsky, and David L. Kaplan. 2016. "Development of a Three-Dimensional Adipose Tissue Model for Studying Embryonic Exposures to Obesogenic Chemicals." *Annals of Biomedical Engineering*, November, 1–12. doi:10.1007/s10439-016-1752-x.

Weisberg, Stuart P., Daniel McCann, Manisha Desai, Michael Rosenbaum, Rudolph L. Leibel, and Anthony W. Ferrante. 2003. "Obesity Is Associated with Macrophage Accumulation in Adipose Tissue." *The Journal of Clinical Investigation* 112 (12): 1796–1808. doi:10.1172/JCI19246.

Wellen, Kathryn E., and Gökhan S. Hotamisligil. 2003. "Obesity-Induced Inflammatory Changes in Adipose Tissue." *Journal of Clinical Investigation* 112 (12): 1785–88. doi:10.1172/JCI200320514.

Wronska, A., and Z. Kmiec. 2012. "Structural and Biochemical Characteristics of Various White Adipose Tissue Depots." *Acta Physiologica* 205 (2): 194–208. doi:10.1111/j.1748-1716.2012.02409.x.

Xu, Haiyan, Glenn T. Barnes, Qing Yang, Guo Tan, Daseng Yang, Chieh J. Chou, Jason Sole, et al. 2003. "Chronic Inflammation in Fat Plays a Crucial Role in the Development of Obesity-Related Insulin Resistance." *The Journal of Clinical Investigation* 112 (12): 1821–30. doi:10.1172/JCI19451.

Yang, Shoufeng, Kah-Fai Leong, Zhaohui Du, and Chee-Kai Chua. 2001. "The Design of Scaffolds for Use in Tissue Engineering. Part I. Traditional Factors." *Tissue Engineering* 7 (6): 679–89. doi:10.1089/107632701753337645.

Zhang, H. H., S. Kumar, A. H. Barnett, and M. C. Eggo. 2000. "Ceiling Culture of Mature Human Adipocytes: Use in Studies of Adipocyte Functions." *Journal of Endocrinology* 164 (2): 119–28. doi:10.1677/joe.0.1640119.

Zhang, Hui H., Melanie Halbleib, Faiyaz Ahmad, Vincent C. Manganiello, and Andrew S. Greenberg. 2002. "Tumor Necrosis Factor-α Stimulates Lipolysis in Differentiated Human Adipocytes Through Activation of Extracellular Signal-Related Kinase and Elevation of Intracellular cAMP." *Diabetes* 51 (10): 2929–35. doi:10.2337/diabetes.51.10.2929.